RESEARCH

Experimental study on the interrelation of multiple mechanical parameters in overburden rock caving process during coal mining in longwall panel

Daixin Deng[1] · Hongwei Wang[1,2] · Lili Xie[1] · Zeliang Wang[1] · Jiaqi Song[1]

Abstract

In order to comprehend the dynamic disaster mechanism induced by overburden rock caving during the advancement of a coal mining face, a physical simulation model is constructed basing on the geological condition of the 21221 mining face at Qianqiu coal mine in Henan Province, China. This study established, a comprehensive monitoring system to investigate the interrelations and evolutionary characteristics among multiple mechanical parameters, including mining-induced stress, displacement, temperature, and acoustic emission events during overburden rock caving. It is suggested that, despite the uniformity of the overburden rock caving interval, the main characteristic of overburden rock lies in its uneven caving strength. The mining-induced stress exhibits a reasonable interrelation with the displacement, temperature, and acoustic emission events of the rock strata. With the advancement of the coal seam, the mining-induced stress undergoes four successive stages: gentle stability, gradual accumulation, high-level mutation, and a return to stability. The variations in other mechanical parameters does not synchronize with the significant changes in mining-induced stress. Before the collapse of overburden rock occurs, rock strata temperature increment decreases and the acoustic emission ringing counts surges with the increase of rock strata displacement and mining-induced stress. Therefore, the collaborative characteristics of mining-induced stress, displacement, temperature, and acoustic emission ringing counts can be identified as the precursor information or overburden rock caving. These results are in good consistent with on-site situation in the coal mine.

Keywords Overburden rock caving · Multiple mechanical parameters · Interrelation characterization · Precursor information

1 Introduction

The roof disaster has the serious hidden danger characteristics of multiple inducing factors, frequent burst and difficulty in prevention and control in various dynamic disasters, the number of occurrence and death toll of roof accidents have always occupied the first place of coal mine dynamic disasters in China for a long time, which is the main problem that affecting coal mine safety production (Alejano et al. 2008; Jiang et al. 2014; Jiang et al. 2015; Yuan et al. 2018; Wang et al. 2020a; Wang et al. 2020b). In general, a sudden and violent caving of overburden rock can release containing deformation energy and cause roof disaster during longwall panel advancement where machinery and workers assemble (Singh et al. 2010; Tsesarsky 2012; Gao et al. 2014a, b; Gong et al. 2016). Therefore, the key to roof disaster prevention and control is to analyze the occurrence characteristics of overburden rock collapse and study the interrelation and evolution characterization of multiple mechanical parameters of rock strata in the process of overburden rock movement.

The multiple mechanical parameters precursor information during coal and rock fracture process have always been continuous hot research (Su et al. 2021; Wang et al. 2021a, b, c; Wang et al. 2022). Li et al. (2019) proposed that the sensitivity priority of precursor information of rock failure is stress, displacement and seepage pressure

✉ Hongwei Wang
whw@cumtb.edu.cn

1 School of Mechanics and Civil Engineering, China University of Mining and Technology, Beijing 100083, China

2 State Key Laboratory of Coal Resources and Safe Mining, China University of Mining and Technology, Beijing 100083, China

basing on the research results of the true triaxial geomechanical model test. Khan et al. (2021) carried out micro-seismic monitoring in Tashan coal mine and presented a novel approach for tracing micro-seismic events and mapping induced fractures to identify and predict dangerous areas that may lead to overburden rock collapse. Ding et al. (2022) explored that the rapid changes of acoustic emission parameters including the dissipated energy, ringing count, RA value, information entropy and acoustic emission damage can be used as the precursor information of rock fracture. Hao et al. (2022) designed infrared monitoring tests of coal and rock instability damage under different crack inclination angles, and stated that infrared precursory information of coal and rock is mostly about 80%–85% of the peak stress or instability time and the horizontal fracture will make the failure precursory appear in advance.

Considerable efforts have been expended to acquire comprehensive research on the occurrence characteristics and the evolution law of overburden rock movement (Zhang et al. 2011; Cheng et al. 2016; Wang et al. 2016). Geological condition such as geological structure, overburden rock strength and thickness, burial depth, mining method, coal seam strength and thickness have a great impact on overburden rock movement behavior (Shan et al. 2016; Li et al. 2017; Amini et al. 2018; Wang et al. 2021b). Liu et al. (2011b) found that the development characteristic of cracks in the overburden rock was that the cracks first expanded from the bottom strata to the upper strata as the collapsed rock strata was gradually compacted during coal seam advancement process. Kumar et al. (2015) pointed that the scale of overburden collapse area and the magnitude of ground subsidence were directly proportional to the mining height and both increased with the increase of mining height, which would greatly affect the goaf behavior. Shen et al. (2016) discussed the influence of main roof five fracture positions on the roadway and found that the fracture position of the roof near the rib in the goaf was the most effective position to guarantee the stability of the roadway. Bai et al. (2017) pointed that the hard rock strata would not collapse immediately after the mining face advancement, but formed a cantilever beam structure suspended above the coal pillar, which could cause the phenomenon of high lateral abutment pressure in the coal pillar. Liu et al. (2019) considered that the dynamic loading was formed by the hard rock strata large area suspension above the shallow buried goaf and the coal seam compression caused by rock strata fracture and rotation movement. Wang et al. (2021a) proposed that the failure process of the hard roof could be divided into three stages including initial stability period, stable movement period and overall collapse period, and the roof movement presented unstable dynamic changes of separation, instantaneous subsidence, separation closure, intermittent stability and instantaneous collapse compaction.

Due to the difficulty to observe the movement and collapse behavior of overburden rock on-site under the advancement condition of the mining face, the physical experiment method is still a common way to explore the characteristics of the overburden rock movement. Liu et al. (2011a) explored the mechanism of roof disasters from the dynamic loading transfer effect of overburden rock damage structure, basing on the analysis of a large number of roof accidents in the advancement process of coal seam. Ghabraie et al. (2015) illustrated that the rock strata movement profile and incremental subsidence could be divided into three different areas after coal seam advancement in physical model, which had different movement characteristics in vertical and horizontal directions. Chen et al. (2019) studied the space–time relationship between the periodic fracture of roof structure and the rebound compression field in the whole region by using the physical experiment method. Ren et al. (2019) analyzed the time series characteristics of multiple parameters in the roof failure process by physical experiment model and pointed that the rock strata was easy to transform from "x" type fracture, strength yield failure to single shear failure.

Basing on the 21221 mining face geological condition of Qianqiu coal mine in Henan Province, China, this paper adopts the physical experiment method, prepares the similarity materials model in the indoor laboratory, arranges a new multiple mechanical parameters monitoring system including mining-induced stress, displacement, temperature and acoustic emission monitoring, simulates the overburden rock deformation and collapse process during the coal seam mining. By analyzing the interrelation and evolution characterization of mining-induced stress, displacement, temperature and acoustic emission of overburden rock collapse stage, the precursor information of overburden rock collapse is summarized. It is beneficial to develop the overburden rock control method in the stope and establish corresponding early warning and prevention technology system, which has significant scientific significance and engineering guiding value for the prevention and control of roof dynamic disasters.

2 Site descriptions

Qianqiu coal mine in Yima coal field covers an area of 17.99 km^2 and locates in Henan Province, China, and it is surrounded in complex geological environment with the existence of large synclines and faults (Xie et al. 2008; Liu et al. 2017). Potou fault, Shanshi-Yima fault and Yima syncline, Zhangcun fault and Shanshen syncline, Anshang strike-slip fault are located at the northern, southern, western and eastern boundary of Qianqiu coal mine respectively (Lv et al. 2014; Wang et al. 2017), as shown in Fig. 1. A large number of faults and synclines lead to intensive stress concentration in Qianqiu coal mine,
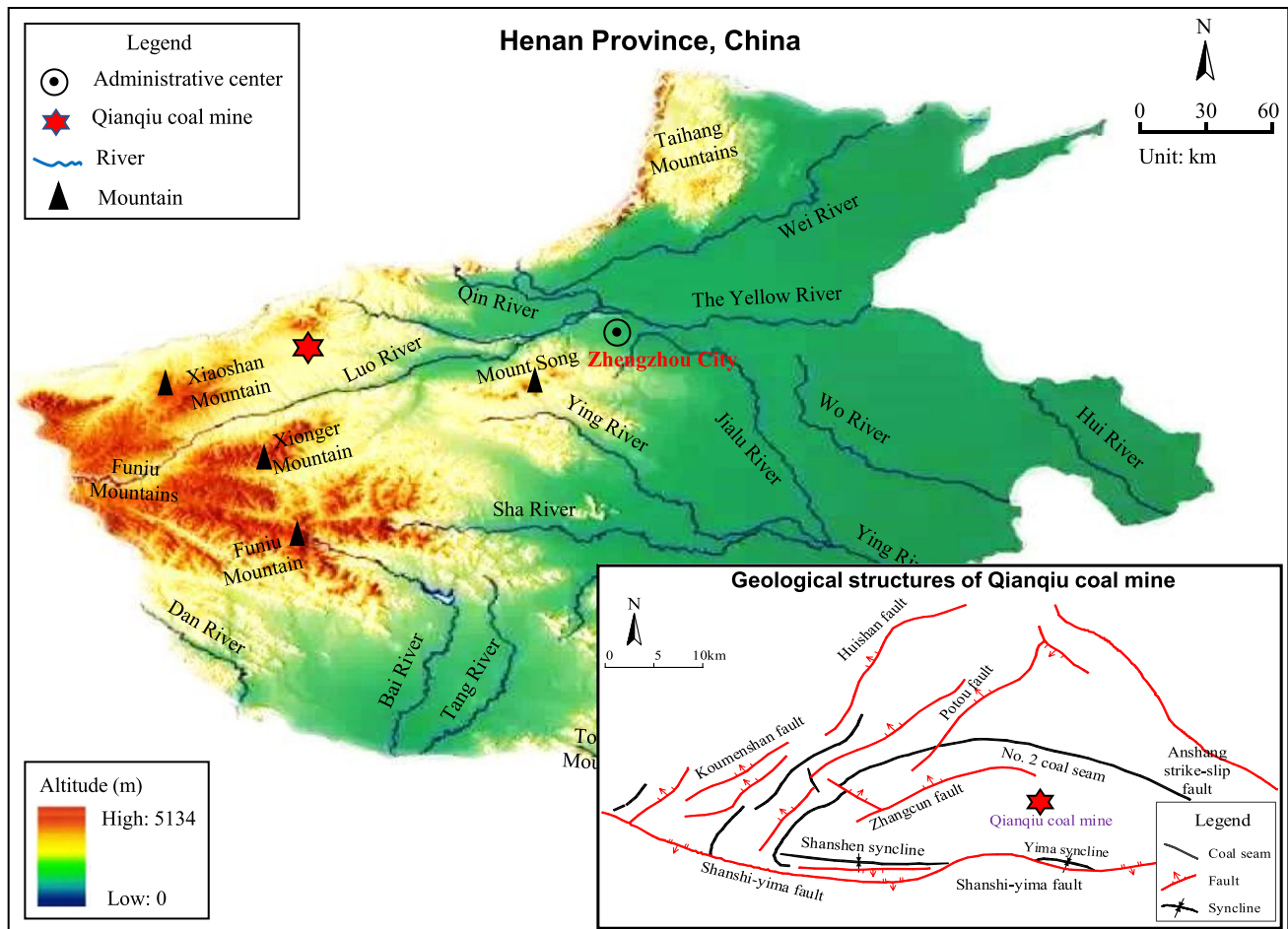
Fig. 1 Location and geological structures of Qianqiu coal mine

which has quite a destructive impact on the prevention and control of dynamic disasters in Qianqiu coal mine.

The main productive coal seam in Qianqiu coal mine is the No.2 coal seam which is cut apart by F_{16} fault (near east–west compressive torsional thrust fault) during its formation and development. 21221 mining face with the longwall mining method is a typical longwall panel. Figure 2 presents mining layout of 21221 longwall panel and the southern boundary of 21221 longwall panel is adjacent to F_{16} fault and its northern boundary is 21201 goaf.

The floor of 21221 longwall panel is siltstone with average thickness of 26 m, the immediate roof is fine sandstone with average thickness of 10 m and the main roof is mudstone with an average thickness of 24 m, whereas overburden rock is conglomerate rock with average thickness of 550 m and uniaxial compressive strength (UCS) of 45 MPa, as shown in Fig. 3. It is known that the typical stratigraphic characteristics of 21221 longwall panel is the occurrence of thick and hard conglomerate rock above coal seam.

3 Physical simulation of overburden rock collapse during coal seam mining

3.1 Physical model construction

The physical experiment takes the geological condition of 21221 longwall panel in Qianqiu coal mine as the geological prototype and uses physical model to study the overburden rock collapse behavior. The similarity materials consist of fine sand, gypsum, lime and water to simulate the actual rock strata in the physical model. These materials are widely treated as aggregates and binder in physical experiments. The current rock mechanics theory and engineering technology cannot make the physical model completely similar to the actual project in terms of various physical and mechanical parameters and constitutive relation. This study mainly considers that main parameters such as uniaxial compressive strength, elastic modulus,
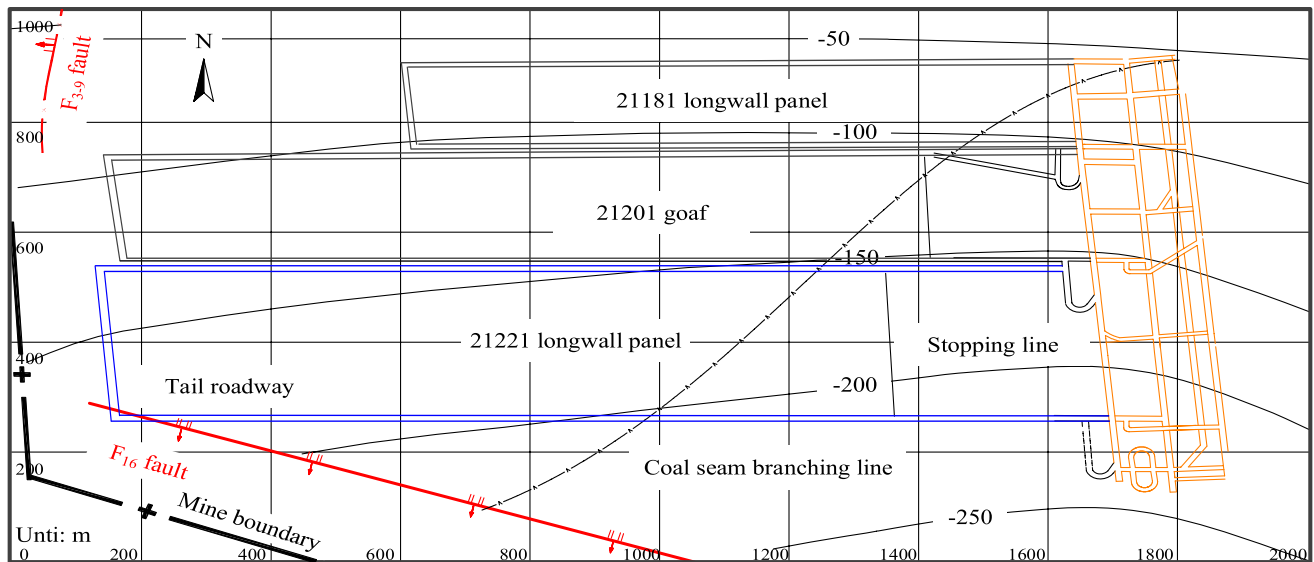
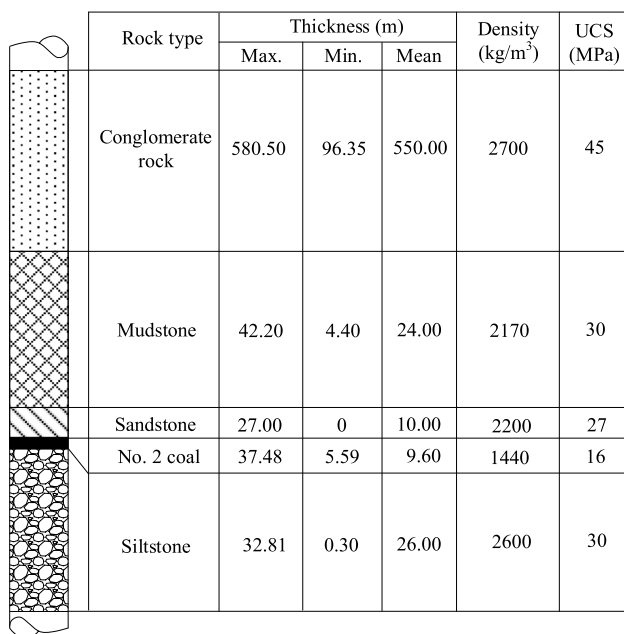**Fig. 2** Mining layout of 21221 longwall panel in Qianqiu coal mine

Fig. 3 Stratigraphic column of 21221 longwall panel in Qianqiu coal mine (Wang et al. 2019)

unit weight and Poisson's ratio meet similarity condition between actual rock strata and similarity materials.

The ratio of the physical quantity with same dimension between the actual project model and the physical model is regarded as the similarity coefficient. According to the similarity criteria (He et al. 2010; Zhu et al. 2011; Sun et al. 2018; Lou et al. 2021), the similarity coefficient of the main parameters is determined by comprehensively considering the physical properties of similarity materials and laboratory condition, as shown in Table 1.

The physical model is built on the experiment platform with the dimensions of 150 cm × 100 cm × 10 cm. Therefore, five layers of rock strata including siltstone, coal seam, sandstone, mudstone and conglomerate rock are made with five mixed proportions and the thickness of rock strata are 13, 6, 6, 24 cm and 51 cm, respectively as shown in Table 2.

Table 3 shows the specific amounts of similarity materials in different proportions used to simulate the rock strata with different strength. Because the experiment mainly studies the deformation and collapse characteristics of the overburden rock under the influence of coal seam mining, the thickness of coal seam and the siltstone on the floor have a small impact

Table 1 Similarity coefficient of model parameters

Geometry	Unit weight	Poisson's ratio	Displacement	Uniaxial compressive strength	Elastic modulus	Boundary stress	Time
$C_L = 100{:}1$	$C_\gamma = 1.6{:}1$	$C_\mu = 1{:}1$	$C_D = 100{:}1$	$C_\sigma = 160{:}1$	$C_E = 160{:}1$	$C_B = 160{:}1$	$C_T = 10{:}1$

Table 2 Parameters of similarity materials

Rock type	Prototype rock			Similarity materials			Fine sand: Gypsum: Lime: Water
	UCS (MPa)	Density (kg/m^3)	Thickness (m)	UCS(MPa)	Density (kg/m^3)	Thickness (cm)	
Conglomerate	44.8	2700	550	0.28	1687	51	6.0:0.5:0.5:0.7
Mudstone	30.4	2170	24	0.19	1356	24	7.0:0.4:0.6:0.8
Sandstone	27.2	2200	10	0.17	1375	6	7.0:0.5:0.5:0.8
Coal seam	16.0	1440	9.6	0.10	900	6	8.0:0.5:0.5:0.8
Siltstone	30.4	2600	26	0.19	1625	13	7.0:0.4:0.6:0.8

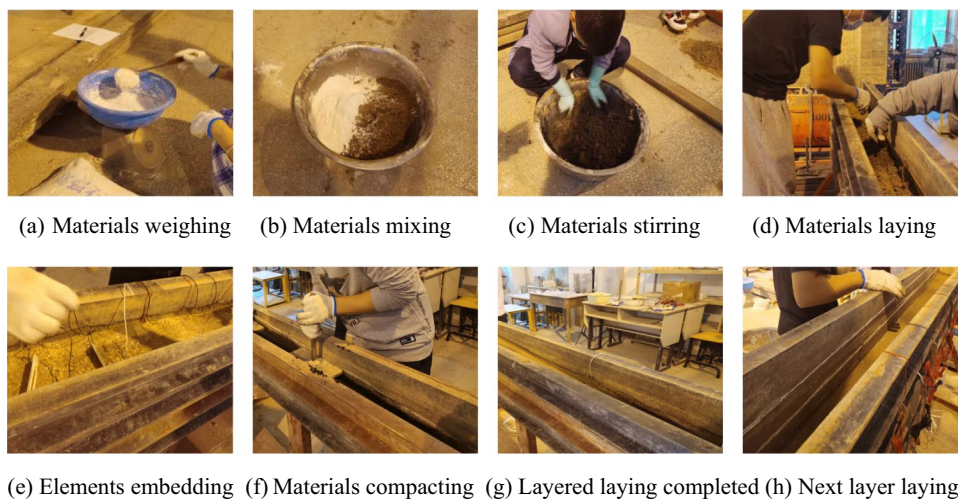**Table 3** The specific amounts of similarity materials in physical model

Rock type	Layering height (cm)	Fine sand (kg)	Gypsum (kg)	Lime (kg)	Water (kg)
Conglomerate	2	7.20	0.60	0.60	0.80
Mudstone	2	7.35	0.42	0.63	0.82
Sandstone	2	7.35	0.52	0.52	0.82
Coal seam	2	7.46	0.47	0.47	0.83
Siltstone	2	7.35	0.42	0.63	0.82

on the overburden rock activity, and in order to lay higher conglomerate as much as possible, the thickness of siltstone, coal seam and sandstone are smaller in the physical model than average thickness in the actual engineering prototype. The UCS of similarity materials in the physical model is closely related to its drying time after the lay completion of physical model. The drying time of similarity materials is seven days in this experiment when similarity materials reach the expected strength. The boundary stress of physical model is loading by hydraulic devices according to the material strength ratio. The

left side, right side, and top side of physical model are loading to 0.13, 0.13, and 0.11 MPa, respectively.
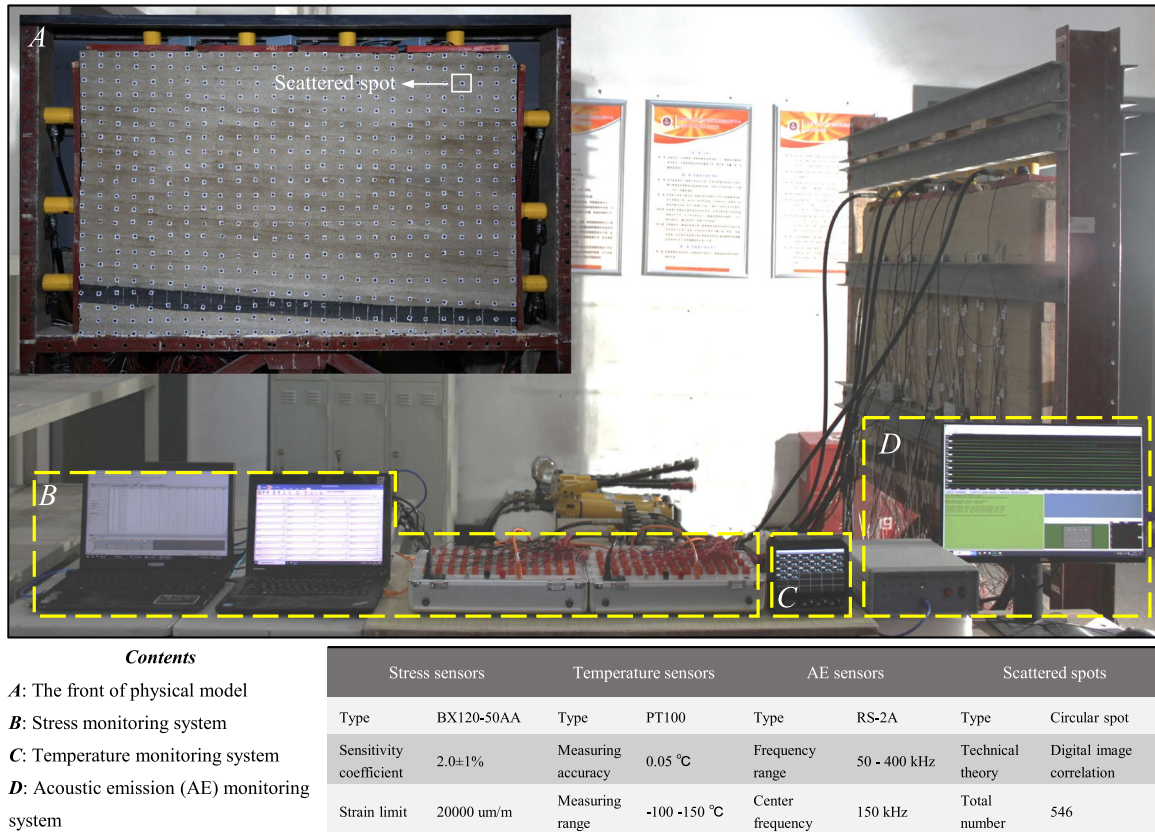
Figure 4 shows the construction process of similarity materials in the physical model, mainly including materials weighing, mixing, stirring, laying and compacting, monitoring elements embedding. Each layer of similarity materials will be sufficiently tamped, it is necessary to prevent damage to the embedded monitoring elements in the physical model during tamping process.

The multiple mechanical parameters monitoring system in physical model includes mining-induced stress monitoring system, deformation monitoring system, temperature monitoring system and acoustic emission (AE) monitoring system. Layout of multiple mechanical parameters monitoring system is shown in Fig. 5. The mining-induced stress monitoring system includes fifty stress sensors, two statical strain indicators and a stress records. The deformation monitoring system is composed of a large number of scattered spots, two lights and a camera. The temperature monitoring system is composed of twenty temperature sensors and a temperature record. The acoustic emission monitoring system manufactured by Softland Times in China (DS5-8A acoustic emission instrument) is composed of eight acoustic

(a) Materials weighing   (b) Materials mixing   (c) Materials stirring   (d) Materials laying

(e) Elements embedding (f) Materials compacting (g) Layered laying completed (h) Next layer laying

Fig. 4 Construction process of similarity materials in physical model

(a) Experiment site layout of multiple mechanical parameters monitoring system

Contents

A: The front of physical model

B: Stress monitoring system

C: Temperature monitoring system

D: Acoustic emission (AE) monitoring system

Stress sensors		Temperature sensors		AE sensors		Scattered spots	
Type	BX120-50AA	Type	PT100	Type	RS-2A	Type	Circular spot
Sensitivity coefficient	2.0±1%	Measuring accuracy	0.05 ℃	Frequency range	50 - 400 kHz	Technical theory	Digital image correlation
Strain limit	20000 um/m	Measuring range	-100 -150 ℃	Center frequency	150 kHz	Total number	546

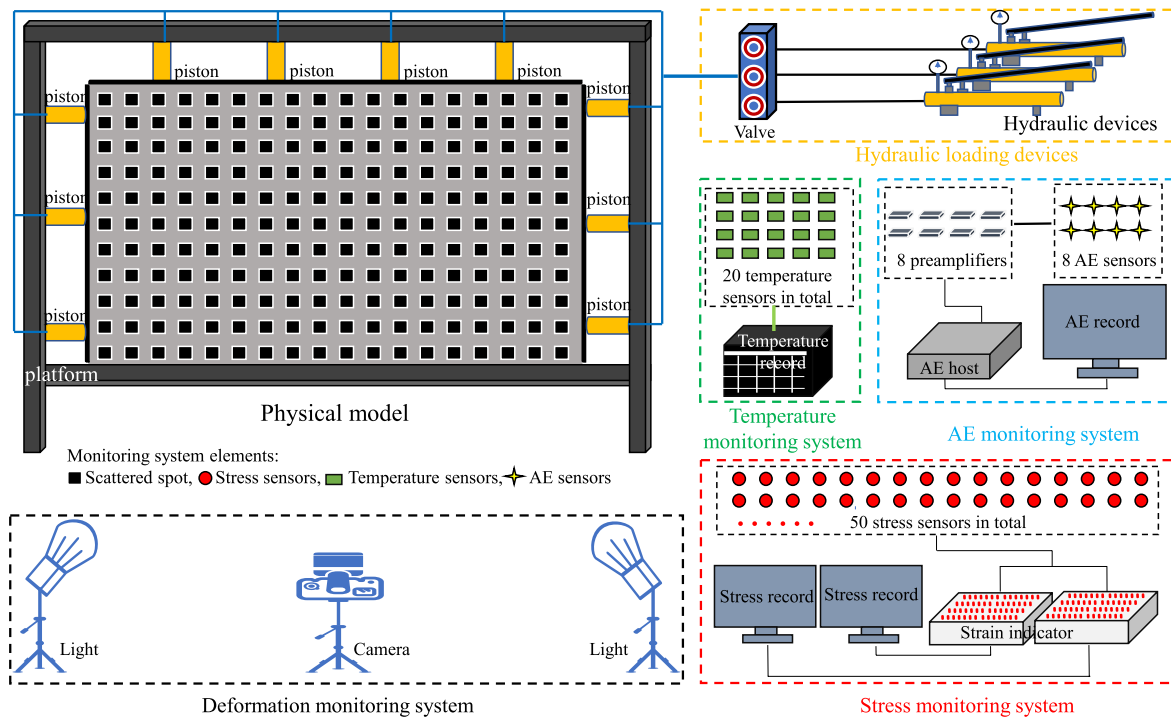## (b) Schematic diagram layout of multiple mechanical parameters monitoring system

Fig. 5 Layout of multiple mechanical parameters monitoring system

emission sensors, eight acoustic emission preamplifiers, an acoustic emission host and a acoustic emission record. Partial parameters of various sensors and scattered spots are presented in Fig. 5. In addition, hydraulic loading devices are used to load on the top side, left side and right side of physical model.

3.2 Multiple mechanical parameters monitoring plan

The monitoring plan in physical model adopts various devices including stress sensors, scattered spots, temperature sensors, acoustic emission sensors to form comprehensive multiple mechanical parameters monitoring methods. It should be noted that stress sensors and temperature sensors are embedded in the physical model during the process of laying similarity materials, acoustic emission sensors are installed behind the physical model and scattered spots are fixed in front of the physical model after the laying process is completed.

3.2.1 Mining-induced stress monitoring

The stress sensor is mainly composed of resistance strain gauge and its specific parameters are shown in Table 4.

The mining-induced stress of overburden rock is monitored by laying stress sensors arranged in six rows in the rock strata. The first row of nine stress sensors in total, numbered correspondingly 1#–9# from left to right, is arranged in the sandstone 4 cm above the coal seam. The second row of nine stress sensors in total, numbered correspondingly 10#–18# from left to right, is arranged in the mudstone 16 cm above the coal seam. The third row of nine stress sensors in total, numbered correspondingly 19#–27# from left to right, is arranged in the conglomerate 28 cm above the coal seam. The fourth row of nine stress sensors in total, numbered correspondingly 28#–36# from left to right, is arranged in the conglomerate 40 cm above the coal seam. The fifth row of nine stress sensors in total, numbered correspondingly 37#–45# from left to right, is arranged in the conglomerate 52 cm above the coal seam. The sixth row of five stress

Table 4 Main parameters of stress sensors

Type	Serial number	Strain limit (um/m)	Sensitivity coefficient	Dimension (mm)	Total sensors
Resistance strain gauge	BX120-50AA	20,000	2.0 ± 1%	50 × 3.0	50

sensors in total, numbered correspondingly 46#–50# from left to right, is arranged in the conglomerate 64 cm above the coal seam. The stress sensors at the left and right ends in each row are 15 cm away from the edges of the physical model, and the two adjacent stress sensors are 12 cm apart in vertical distance and 15 cm apart in horizontal distance (the horizontal spacing between adjacent stress sensors in the sixth row is 30 cm), as shown in Fig. 6.

3.2.2 Overburden rock deformation monitoring

The evolution law of displacement field in the physical model is analyzed by digital target marker image correlation method, and roof displacement monitoring is carried out through tracking a group of the scattered spots (Lin et al. 2013; Mao et al. 2013, 2015; Munoz et al. 2016). The digital target marker image correlation method is based on the principle of digital image correlation method, but it avoids the full-field search in the digital image correlation method and carries on the local area search instead in order to improve the computational speed. The scattered spots on physical model surface are treated as target markers, and will also move and occur displacement with the deformation of rock strata in the physical model. Through image processing correlation algorithms, the change of gray level in the selected area of the scattered spots centroid are tracked to calculate the displacement of the selected area. During the experiment process, the high performance camera and computer are used to continuously collect the deformation image of the model. In order to facilitate scattered spot capture, the camera is adjusted to black and white mode for acquisition. The whole model is arranged with scattered spots. The horizontal distance is 6 cm and the vertical distance is 5 cm in adjacent two scattered spots, as shown in Fig. 6.

3.2.3 Overburden rock temperature monitoring

Platinum resistance temperature sensor is used to monitor temperature and Table 5 shows main parameters of temperature sensor. The temperature change of rock strata in physical model is monitored and reflected in real time through temperature sensors with sensitivity of 0.05 °C. To reduce the impact of experimental environment on temperature monitoring as far as possible, the temperature sensors are buried at a depth of 10 cm along the width of rock strata. A total of twenty temperature sensors are arranged in rock strata in four rows. The five temperature sensors in the first row are arranged in the sandstone 6 cm above the coal seam, and the temperature sensors are numbered correspondingly 1#–5# from left to right. The five temperature sensors in the second row are arranged in the mudstone 26 cm above the

coal seam, and the temperature sensors are numbered correspondingly 6#–10# from left to right. The five temperature sensors in the third row are arranged in the sandstone 46 cm above the coal seam, and the temperature sensors are numbered correspondingly 11#–15# from left to right. The five temperature sensors in the fourth row are arranged in the sandstone 66 cm above the coal seam, and the temperature sensors are numbered correspondingly 16#–20# from left to right. The temperature sensors at the left and right ends in each row are 15 cm away from the left and right edges of the physical model, and the vertical distance is 20 cm and the horizontal distance is 30 cm in adjacent two temperature sensors, as shown in Fig. 6.

3.2.4 Acoustic emission monitoring

The full-information dynamic acoustic emission monitoring system is used to track and accurately locate the fracture evolution process of rock strata under the action of strong mining disturbance. Resonant acoustic emission sensor is an important component of DS5-8A acoustic emission instrument and its specific parameters are shown in Table 6. A total of eight acoustic emission (AE) sensors in two rows are installed in the model. According to the previous experiment experience, when the sensor is mainly arranged in the middle area close to the potential collapse area of the overburden rock in the physical model, the overall monitoring results of
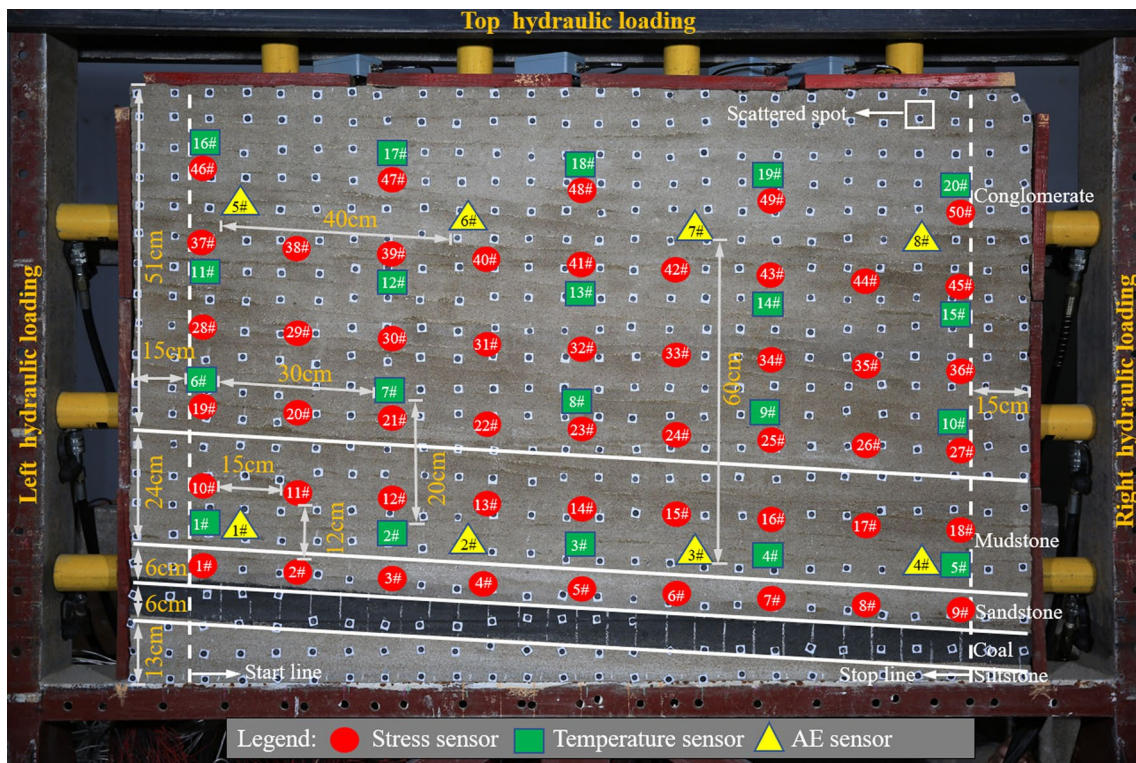

Fig. 6 Layout of multiple mechanical parameters monitoring plan

Table 5 Main parameters of temperature sensors

Type	Serial number	Diameter (mm)	Length (mm)	Resistance change rate (Ω/°C)	Measuring range (°C)	Accuracy (°C)	Total sensors
Platinum Resistance	PT100	5	50	0.3851	− 100 to 150	0.05	20

Table 6 Main parameters of acoustic emission sensors

Type	Serial number	Diameter (mm)	Height (mm)	Frequency range (kHz)	Center frequency (kHz)	Total sensors
Resonant	RS-2A	18.8	15	15–400	150	8

acoustic emission may be good. The four acoustic emission sensors in the first row numbered correspondingly 1#–4# from left to right are arranged in the sandstone 6 cm above the coal seam. The four acoustic emission sensors in the second row numbered correspondingly 5#–8# from left to right are arranged in the conglomerate 66 cm above the coal seam. The acoustic emission sensors at the left and right ends in each row are 15 cm away from the left and right edges of the physical model, and the vertical distance is 60 cm and the horizontal distance is 40 cm between adjacent two acoustic emission sensors, as shown in Fig. 6. It is necessary to measure the propagation velocity of acoustic emission signals from similarity materials to achieve the location of acoustic emission events. The velocity of acoustic emission signals is usually measured by the method of cutting lead material. Due to the complex structure of similarity materials in the physical model, it is mainly manifested that similar materials are soft in the horizontal direction and discontinuous separated by mica powders in the vertical direction, the propagation of acoustic emission signals is complicated and the velocity is uneven in different direction.

3.3 Model experiment results

3.3.1 Movement characterization of overburden rock

The average advancing length is 5 m each step under normal mining condition according to the field data. Therefore, the coal seam is mined 5 cm at each step in the physical model. During the advancement process of the mining face, the whole overburden movement process is photographed with a high performance digital camera and the periodic collapse form of rock strata can be clearly observed. The collapse processes of overburden rock experienced seven stages, as shown in Fig. 7.

(1)	The mining face advances to 50 cm (corresponding 50 m on-site).

When the mining face advances to 50 cm, the first stage of rock strata collapse occurs (Fig. 7b), and the collapse height is 2 cm, the collapse boundary line is shown by the orange line (Fig. 7i). The collapse boundary lines at the left and right ends of the rock strata indicate that the failure form of the rock strata is shear failure. There is horizontal separation fracture above the collapse area, indicating the separation and subsidence of the roof occurs. This is because the deformation state of the roof at this time can be regarded as the flexural deformation of the fixed beam (Shabanimashcool 2015; Liao et al. 2020). One end of the fixed beam is composed of the rock layer above the right coal wall of mining face, and the other end is composed of the rock layer above the left coal pillar, which is consist-

ent with the fixed beam hypothesis theory proposed by Song Zhenqi and Qian Minggao (Qian et al. 2019; Song et al. 2019).

(2)	The mining face advances to 60 cm (corresponding 60 m on-site).

When the mining face continues advancing 10 cm, the second stage of rock strata collapse occurs (Fig. 7c), and the collapse height is 8 cm, the collapse boundary line is shown by the green line (Fig. 7i). The overall boundary of rock strata collapse shows that the failure forms of rock strata are tension failure and shear failure. Due to the influence of the first stage of rock strata collapse, the fractured rock strata above the first stage collapse of rock strata shows tensile failure and shear failure. However, the fractured rock mass above the mining face is shear failure, the deformation state of the roof can be regarded as the shear failure of the statically indeterminate beam. When the collapsed rock strata fully damage and expand, it can provide vertical upward support for the roof. The simply supported end of the statically indeterminate beam is composed of the overhanging rock strata close to the goaf, and the fixed end is composed of the rock strata above the right coal wall.

(3)	The mining face advances to 70 cm (corresponding 70 m on-site).

When the mining face continues advancing 10 cm, the third stage of rock strata collapse occurs (Fig. 7d), and the collapse height is 16 cm, the collapse boundary line is shown by the light pink line (Fig. 7i). The collapse scope in this stage is much larger than that in the previous two collapse stages. This is because the advancement length of mining face has reached 70 cm, the roof overhang length and the influence of gravity have gradually increased, and the roof shows a series of deformation phenomena including bending, sinking and separation. When rock stratum reaches its ultimate bearing capacity under the combined effect of overburden pressure, mining disturbance and gravity, the large failure and collapse of rock strata will occur.

(4)	The mining face advances to 85 cm (corresponding 85 m on-site).

When the mining face continues advancing 15 cm, the fourth stage of rock strata collapse occurs (Fig. 7e), and the collapse height is 16 cm higher than that in the third stage, the collapse boundary line is shown by the bright blue line (Fig. 7i). The collapse scope in this stage is larger than that in the third stage, indicating that overburden rock is more strongly affected by the combined effect of overburden pressure, mining disturbance and gravity. Due to the loss of the support of the lower rock strata, the upper rock strata show rotate and
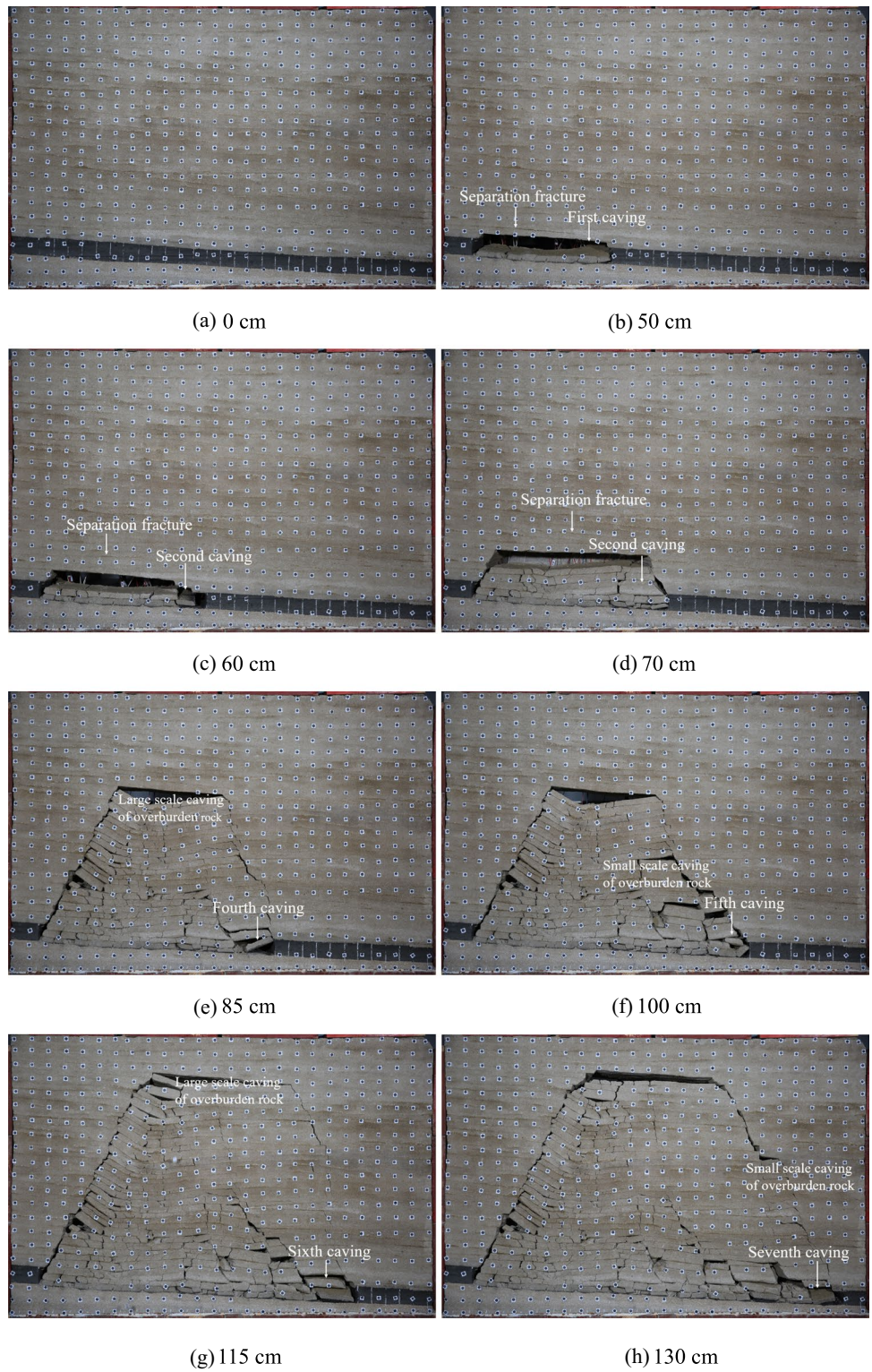
(a) 0 cm

(b) 50 cm

(c) 60 cm

(d) 70 cm

(e) 85 cm

(f) 100 cm

(g) 115 cm

(h) 130 cm

Fig. 7 The movement state of overburden rock during coal seam mining in physical model

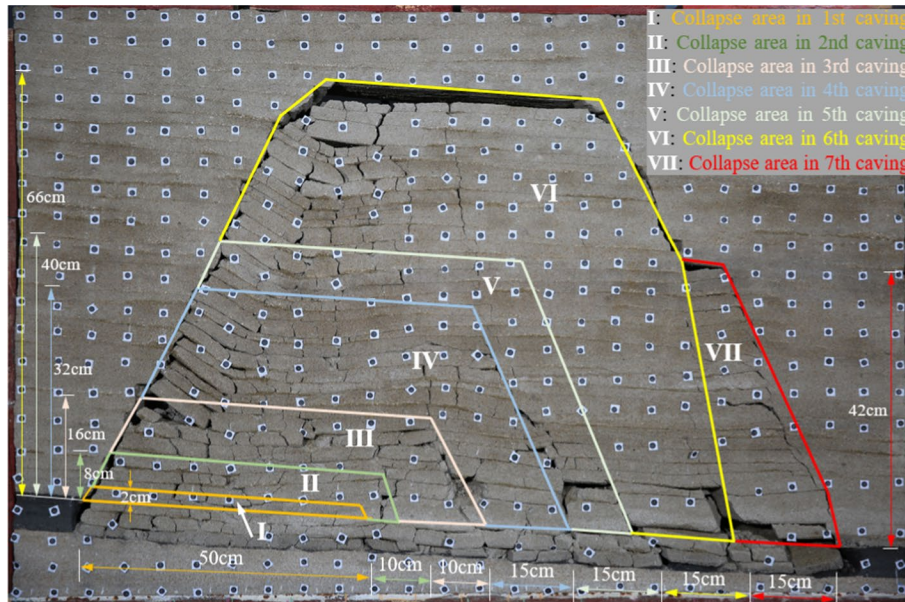(i) Spatial distribution of collapse area in different caving stage

Fig. 7 (continued)

sink due to shear failure and tensile failure, resulting in a large range collapse of overburden rock.

(5) The mining face advances to 100 cm (corresponding 100 m on-site).

When the mining face continues advancing 15 cm, the fifth stage of rock strata collapse occurs (Fig. 7f), and the collapse height is 8 cm higher than that in the fourth stage, the collapse boundary line is shown by the light green line (Fig. 7i). At this stage the collapse scope is small, mainly located in the lower rock strata above the mining face. At this time, the deformation state of rock strata obviously conforms to the shear fracture of the statically indeterminate beam.

(6) The mining face advances to 115 cm (corresponding 115 m on-site).

When the mining face continues advancing 15 cm, the sixth stage of rock strata collapse occurs (Fig. 7g), and the collapse height is 26 cm higher than that in the fourth stage, the overall collapse height reaches 72 cm, the collapse boundary line is shown by the yellow line (Fig. 7i). In this stage the collapse scope has reached the maximum range and strong ground pressure behavior has occurred from the collapsed rock strata, which will have a significant effect on the mining face.

(7) The mining face advances to 130 cm (corresponding 130 m on-site).

When the mining face continues advancing 15 cm, the seventh stage of rock strata collapse occurs (Fig. 7h), and the collapse height is 42 cm, the collapse boundary line is shown by the red line (Fig. 7i).

The collapse scope above the mining face in this stage is smaller than that in sixth stage. At this stage, the deformation state of rock strata also conforms to the shear fracture of the statically indeterminate beam.
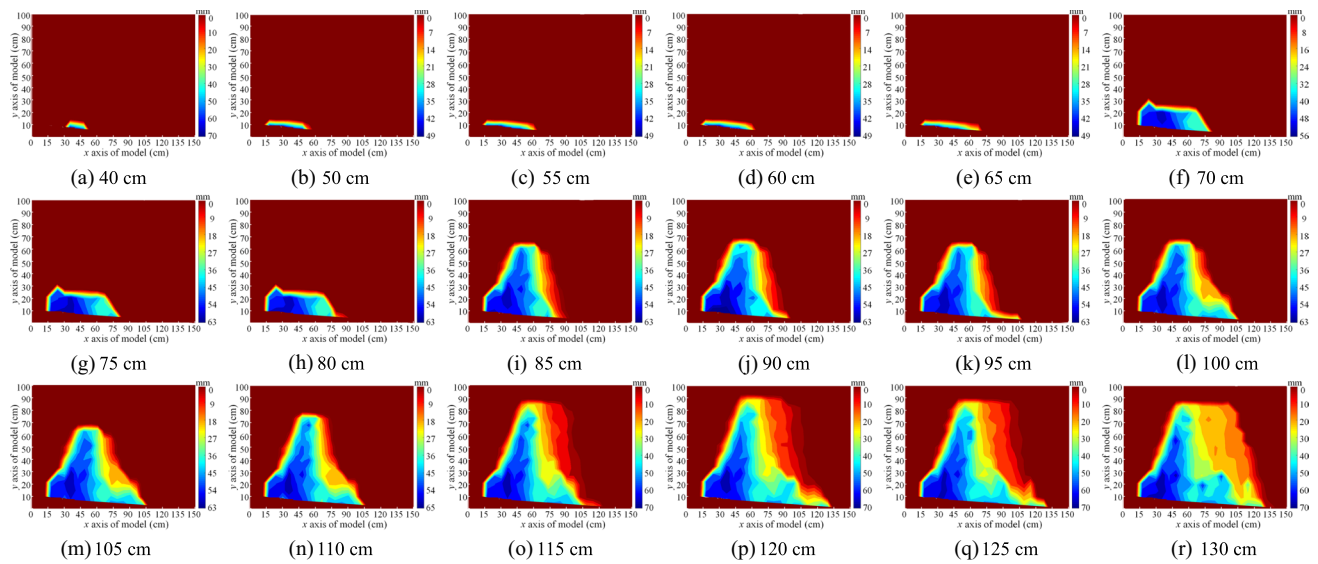
The failure form of rock strata are tension failure and shear failure in seven stages of rock strata collapse. The stepped shear failure occurs at the collapse boundary lines in the left and right ends, which is mainly subjected to the influence of bedding. Except for the first stage of rock strata collapse, the advancement length of the mining face is 10 cm or 15 cm when the rock strata occur collapse in the following six stages. Although overburden rock weighting interval is nearly uniform, the main characteristics of overburden rock caving are uneven weighting strength.

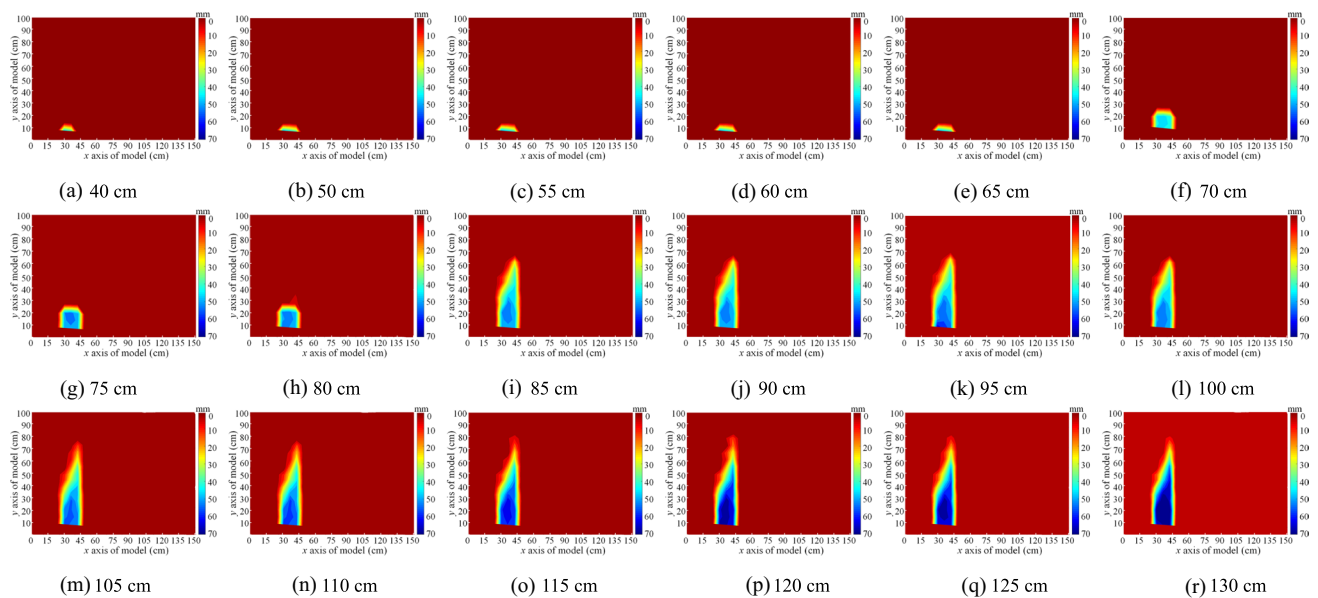### 3.3.2 Displacement evolution characterization of overburden rock

To further illustrate the characteristics of overburden rock movement, Fig. 8 shows displacement variation of overburden rock processed using the digital target marker image correlation method as the mining face advancement in the experiment, including displacement contour (Fig. 8a), displacement in a 20 cm wide band zone along vertical direction (Fig. 8b) and displacement in a 25 cm wide band zone along horizontal direction (Fig. 8c).

When the mining face advances to 60 cm, the overburden rock are slightly disturbed and gradually appear small

(a) Overburden rock displacement contour

(a) 40 cm   (b) 50 cm   (c) 55 cm   (d) 60 cm   (e) 65 cm   (f) 70 cm

(g) 75 cm   (h) 80 cm   (i) 85 cm   (j) 90 cm   (k) 95 cm   (l) 100 cm

(m) 105 cm   (n) 110 cm   (o) 115 cm   (p) 120 cm   (q) 125 cm   (r) 130 cm

(b) Overburden rock displacement in a 20 cm wide band zone along vertical direction

(a) 40 cm   (b) 50 cm   (c) 55 cm   (d) 60 cm   (e) 65 cm   (f) 70 cm

(g) 75 cm   (h) 80 cm   (i) 85 cm   (j) 90 cm   (k) 95 cm   (l) 100 cm

(m) 105 cm   (n) 110 cm   (o) 115 cm   (p) 120 cm   (q) 125 cm   (r) 130 cm

Fig. 8 Displacement variation of overburden rock during coal seam mining

scope displacement. There are two large scope collapses of overburden rock when the mining face advances to 85 cm and the movement of rock strata is relatively strong, the displacement evolution area expands rapidly to the upper of overburden rock. With the continuous advancement of mining face, the height of rock strata collapse reaches the maximum and the evolution height of overburden rock displacement slowly increases, but the evolution width of overburden rock displacement continues to rapidly increase. The evolution width of overburden rock displacement reaches the maximum when the mining face advances to 130 cm.

The nonlinear dynamic displacement can be observed from overburden rock local static deformation to overburden rock overall violent collapse, as shown in Fig. 8a. It can be seen that the displacement of overburden rock at the left side of the model is larger than that at other positions. To further analyze rock mass displacement evolution process, Fig. 8b, c present displacement in specific zone along vertical direction and horizontal direction respectively, it can be seen that when the mining face advances to 85 cm, the overburden rock displacement suddenly increases.

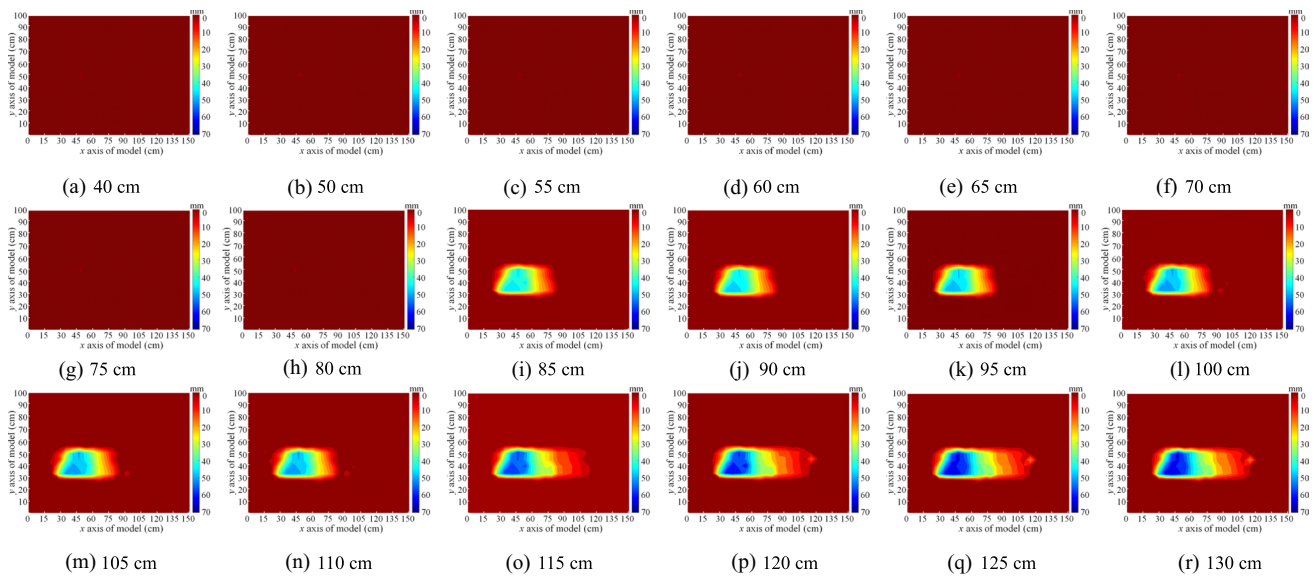(c) Overburden rock displacement in a 25 cm wide band zone along horizontal direction

(a) 40 cm	(b) 50 cm	(c) 55 cm	(d) 60 cm	(e) 65 cm	(f) 70 cm

(g) 75 cm	(h) 80 cm	(i) 85 cm	(j) 90 cm	(k) 95 cm	(l) 100 cm

(m) 105 cm	(n) 110 cm	(o) 115 cm	(p) 120 cm	(q) 125 cm	(r) 130 cm

Fig. 8 (continued)

3.3.3 Mining-induced stress distribution characterization of overburden rock

It is significant to describe overburden rock mining-induced stress characteristics of the specific zone in Figs. 8b, c. It should be noted that the data recorded from the stress sensor is the strain value. The stress value can be obtained through a linear stress–strain relationship of stress sensors. Therefore, this study uses the strain value measured by the sensor to analyze the mining-induced stress of overburden rock, as shown in Fig. 9.

There are 11 stress sensors in the same specific zone in Fig. 8b, and the 11 stress sensors can be divided into three small areas, as shown in Fig. 9a. It can be found that the mining-induced stress in the same small area has the synchronous evolution characteristics, and the mining-induced stress in different small areas has different characteristics. The mining-induced stress mainly shows three different evolution characteristics including first sharp increase and then sudden drop, first slow increase and then sudden increase, always slow increases, as shown in Fig. 9a. With the transmission of mining-induced stress in the advancement process of mining face, the mining-induced stress of rock strata near the goaf has experienced four stages including gentle stability, gradual accumulation, high-level mutation and returning to stability. There are 18 stress sensors in the same specific zone in Fig. 8c, and the 18 stress sensors can be divided into three small areas, as shown in Fig. 9b. It can be found that the mining-induced stress in the same small area has the synchronous change characteristics, and the mining-induced stress in different small areas also has same change characteristics. The change characteristics of mining-induced stress mainly shows first slow increase and then sudden increase, as shown in Fig. 9b, and it can be seen that when the mining face advances to 85 cm, the mining-induced stress occurs sudden increase, which has a good correspondence with the displacement change. In addition, Fig. 9c presents the mining-induced stress variation of overburden rock in other areas, each of three stress sensors including 4#–6# stress sensors and 7#–9# show the same variation trend of mining-induced stress. The mining-induced stress of 4#–6# and 7#–9# stress sensors show dramatical increase when the mining face advances to 70 cm and 100 cm, respectively. The overall mining-induced stress variation of 32#, 33#, 40#–42#, 48# stress sensors is fluctuating and slowly increases. However, when the mining face advances to 110 cm, the mining-induced stress variation of 35#, 36#, 44#, 45#, 49#, 50# stress sensors show rapid reduction.

It is precisely because of the internal mechanism of the transmission and rebalancing of mining-induced stress, combined with the seven caving stages of overburden rock, mining-induced stress shows gentle stability where it is less affected by mining disturbance and the second stage of rock stratum caving occurs; mining-induced stress presents gradual accumulation then high-level mutation where it is greatly affected by mining disturbance and rock strata occur collapse in a large range from the third stage to the sixth stage; mining-induced stress is returning to stability where it is less affected by mining disturbance and the seventh stage of rock stratum caving occurs.

(a) The mining-induced stress variation of overburden rock along vertical direction
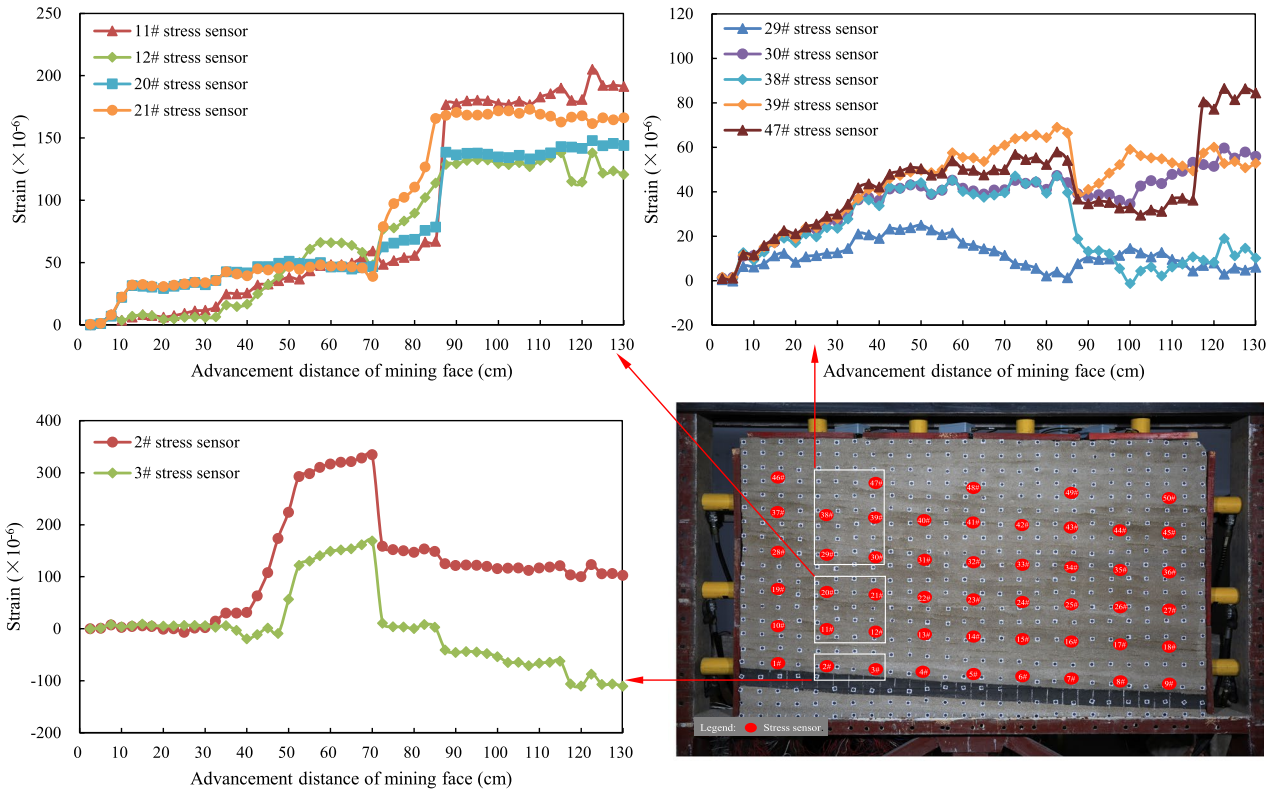
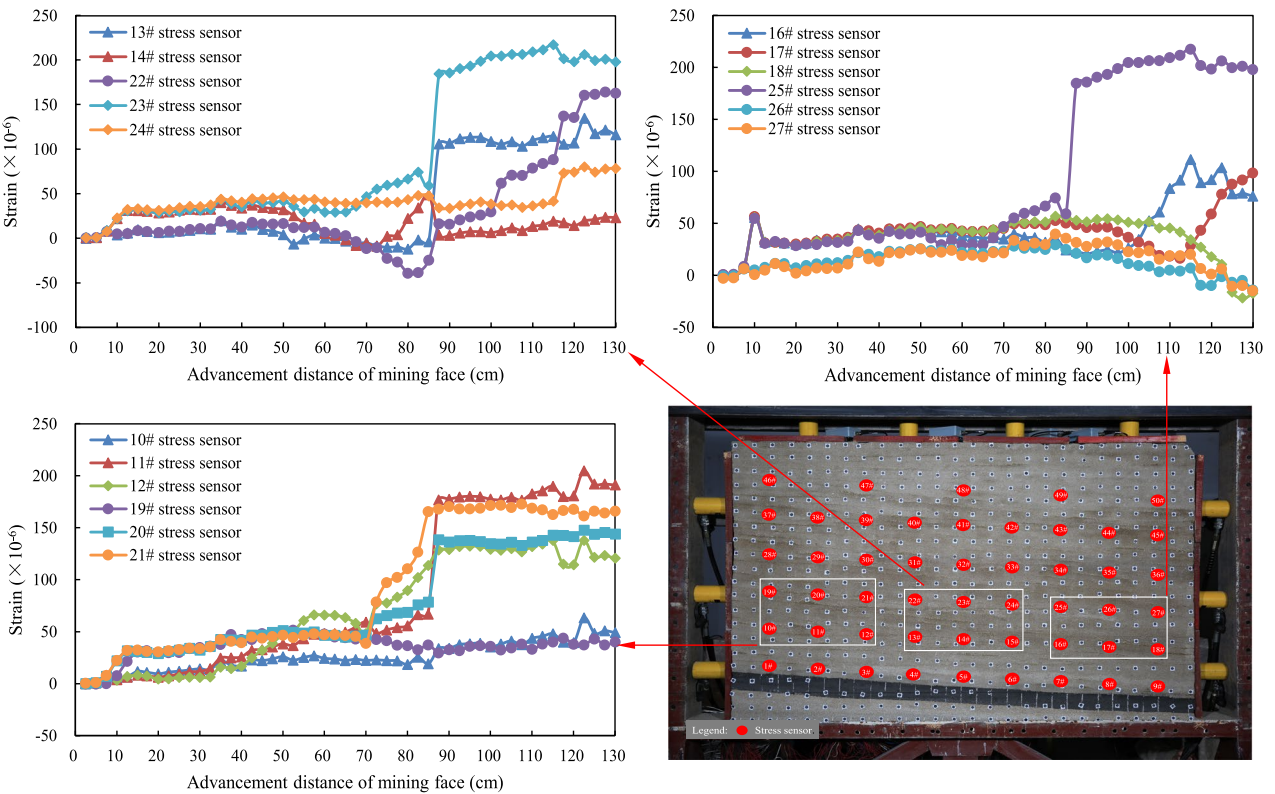(b) The mining-induced stress variation of overburden rock along horizontal direction

Fig. 9 The mining-induced stress variation of different overburden rock areas during coal seam mining

(c) The mining-induced stress variation of overburden rock in other areas
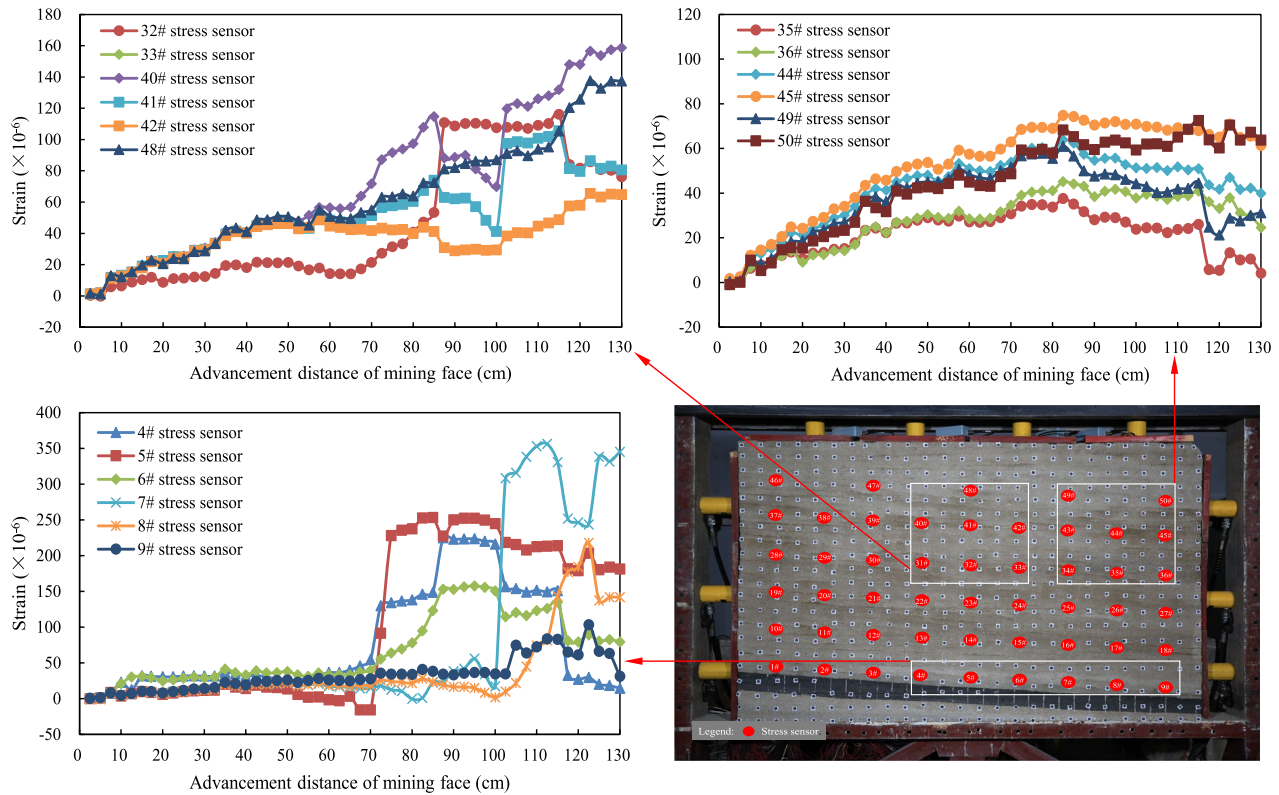

Fig. 9 (continued)

From the above analysis, it can be found that the mining-induced stress has different characteristics along different directions. In the horizontal direction, the mining-induced stress has the same change characteristics in the whole area; in the horizontal direction, the mining-induced stress has the synchronous change characteristics in the small area.

3.3.4 Spatial distribution characterization of acoustic emission events in overburden rock

Acoustic emission event is the simplest indicator of rock micro fracture. Eight acoustic emission sensors detect micro fracture within a specified duration to obtain cumulative acoustic emission events in order to obtain better location results of acoustic emission sources, it should need to measure the transverse wave velocity and longitudinal wave velocity of acoustic emission signals respectively. The transverse wave velocity, longitudinal wave velocity measurement results by cutting lead material are 915, 775 m/s respectively. Based on acquired velocity of acoustic emission signals, the other positioning parameters in the acoustic emission analysis software are selecting repeatedly, and the accurate and reasonable location results of acoustic emission events from similarity materials during the advancement process of

mining face are obtained. The number of acoustic emission events gradually increases with the increase of advancement distance. The horizontal coordinate (x axis) and vertical coordinate (y axis) in the Fig. 10 are the length and height of the similarity model, respectively. The ball with different colors correspondingly represents the acoustic emission events in different stages of different strength roof collapse.

As the advancement distance of the mining face is from 0 to 130 cm, there are seven stages of rock strata collapse during the whole mining period. The spatial distribution of acoustic emission events in seven stages of rock strata collapse is shown in Fig. 10. The overburden fracture is represented by the ball position and the energy of acoustic emission events is represented by the ball diameter in the figure. Two pieces of messages can be obtained from the distribution characteristics of acoustic emission events. Firstly, the amount of acoustic emission events is positively correlated with the scope of rock strata collapse. For example, a small number of acoustic emission events are obtained from small scope stage of rock strata collapse, such as the first stage, the second stage, the third stage and the fifth stage (Figs. 10b–f). In addition, a large number of acoustic emissions events are obtained from large scope stage of rock strata collapse, such as the fourth stage, the sixth stage
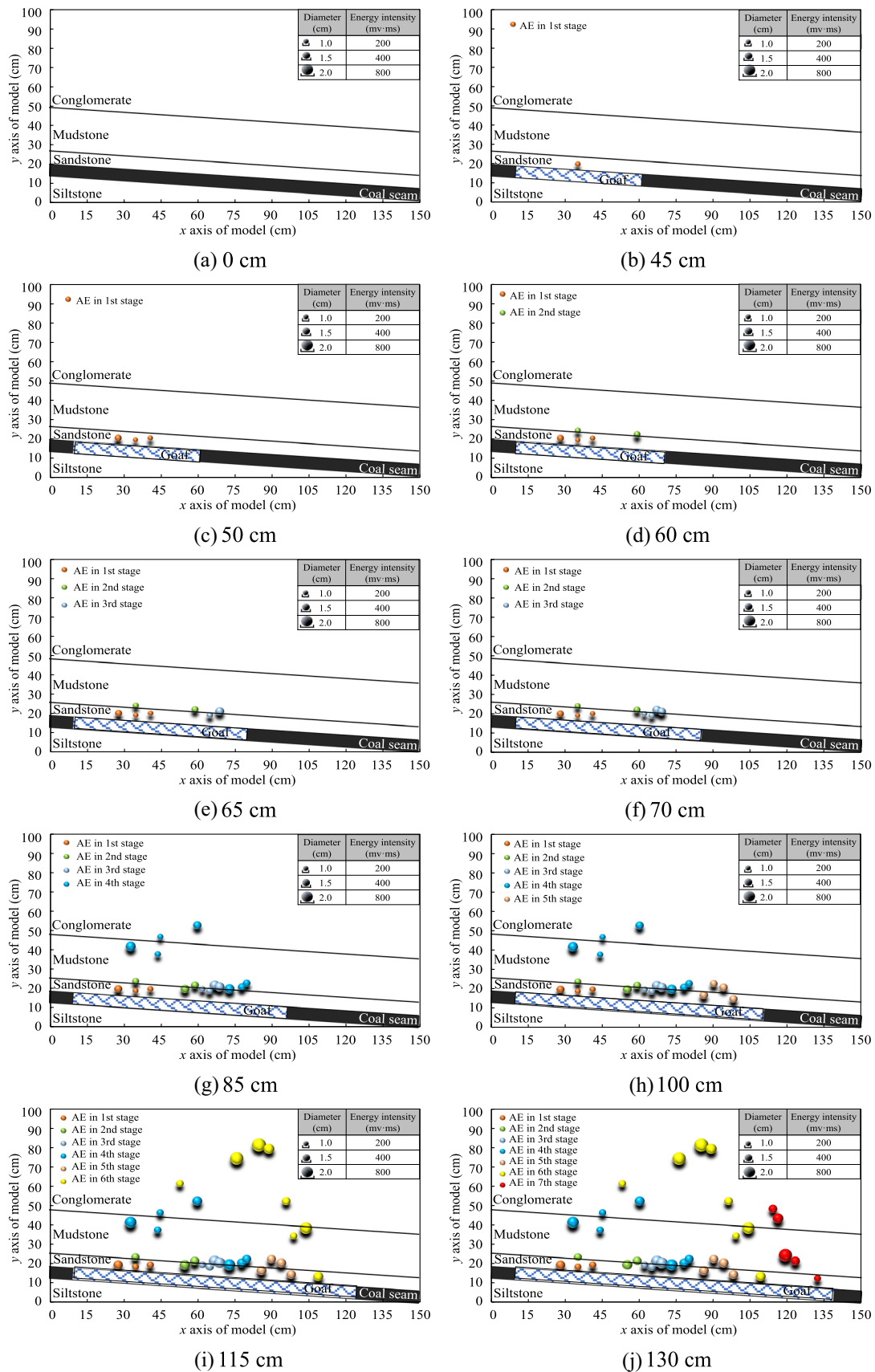
(a) 0 cm

(b) 45 cm

(c) 50 cm

(d) 60 cm

(e) 65 cm

(f) 70 cm

(g) 85 cm

(h) 100 cm

(i) 115 cm

(j) 130 cm

Fig. 10 Spatial distribution of AE events in seven stages of rock stratum collapse

Table 7 The parameters of acoustic emission events during coal seam advancement

Advancement distance (cm)	Total AE counts	Cumulative AE events	Cumulative energy of AE events (mv ms)
0	0	0	0
45	5	1	211
50	6	3	831
60	11	5	1489
65	19	7	2401
70	25	10	3238
85	49	18	6581
100	63	22	8179
115	152	29	12,256
130	173	35	14,496

and the seventh stage (Figs. 10e, g, h). Secondly, most of acoustic emissions events with high energy are recorded in extra-thick conglomerate (Fig. 10g). The location of acoustic emission events is basically consistent with the position of rock fracture. Table 7 shows the parameters of acoustic emission events during coal seam advancement.

The maximum energy of acoustic emission events occurs at hard conglomerate fracture, indicating that the failure strength of hard conglomerate is extremely high. This is due to under the influence of mining disturbance, the bending deformation of hard conglomerate gradually increases and it is easy to accumulate a large amount of deformation energy.

3.3.5 Temperature evolution characterization of overburden rock

The physical experiment continues 2 h and 10 min, and the indoor temperature is basically stable, the temperature change of overburden rock has little influence from indoor temperature. The rock temperature is basically consistent with the room temperature before coal seam mining. In addition, the change characteristic of overburden rock temperature is analyzed by taking the relative change amount of temperature to minimize the impact of environmental temperature change. As the advancement of the mining face, the temperature increment of 20 temperature sensors in four rows located in the overburden rock are shown in Fig. 11.

Figure 11 presents the temperature change of rock mass at different position in the seven stages of rock strata collapse. It can be seen that when the mining face advances to 60 cm, due to the influence of coal seam mining disturbance, the temperature of rock strata at a distance of 6 cm above the coal seam increases slowly and the second stage

of rock strata collapse occurs. The mining face continues advancing to 80 cm, corresponding to before the fourth stage of rock strata collapse, the temperature of 1#–3# temperature sensors sharply decrease and the maximum reduction is 0.8 °C (Fig. 11a). When the mining face advances to 100 cm, the temperature of rock strata at a distance of 26 cm above the coal seam increases slowly, but the temperature of 8# temperature sensor decreases rapidly where the mining face advances to 120 cm, which corresponds to after the sixth stage of rock strata collapse (Fig. 11b). The advancement of the mining face is between 85 and 105 cm, the temperature of 12#, 13# temperature sensors in the rock strata at a distance of 46 cm above the coal seam sharply decreases and the maximum reduction is 0.4 °C. However, when the advancement of the mining face is between 105 and 130 cm, the temperature of 12#, 13# temperature sensors increase rapidly and the maximum temperature rise is 0.3 °C (Fig. 11c). During the whole advancement period of the mining face, the temperature of rock strata at a distance of 66 cm above the coal seam remained gradually increasing after short stability stage (Fig. 11d).

The temperature evolution of rock strata has obvious stage characteristics and the maximum increase and reduction of temperature change are 0.3 °C and 0.8 °C respectively. The temperature of overburden rock gradually increases with the advancement of mining face, which is due to the deformation energy accumulation caused by the bending deformation of the overburden rock. Subsequently, overburden rock occurs collapse several times and the deformation energy quickly release, leading to a significant decrease in the rock strata temperature. Therefore, the temperature of overburden rock has obvious response characteristics for the deformation and failure of overburden rock.

4 Discussion

Although overburden rock collapse has the characteristics of sudden occurrence, it obviously needs the evolution process from stable state to final collapse state, and it is significant to understand the coordinated change of multiple mechanical parameters in the overburden rock collapse process for scientific prevention and control of roof disaster. It is believed that stress state is the essential factor that leads to sudden instability and collapse of rock strata (Shen et al. 2008; Dou et al. 2014; Qi et al. 2019). Therefore, this section focuses on analyzing the interrelation between mining-induced stress and displacement, temperature, acoustic emission of overburden rock caving during coal seam mining in longwall panel.
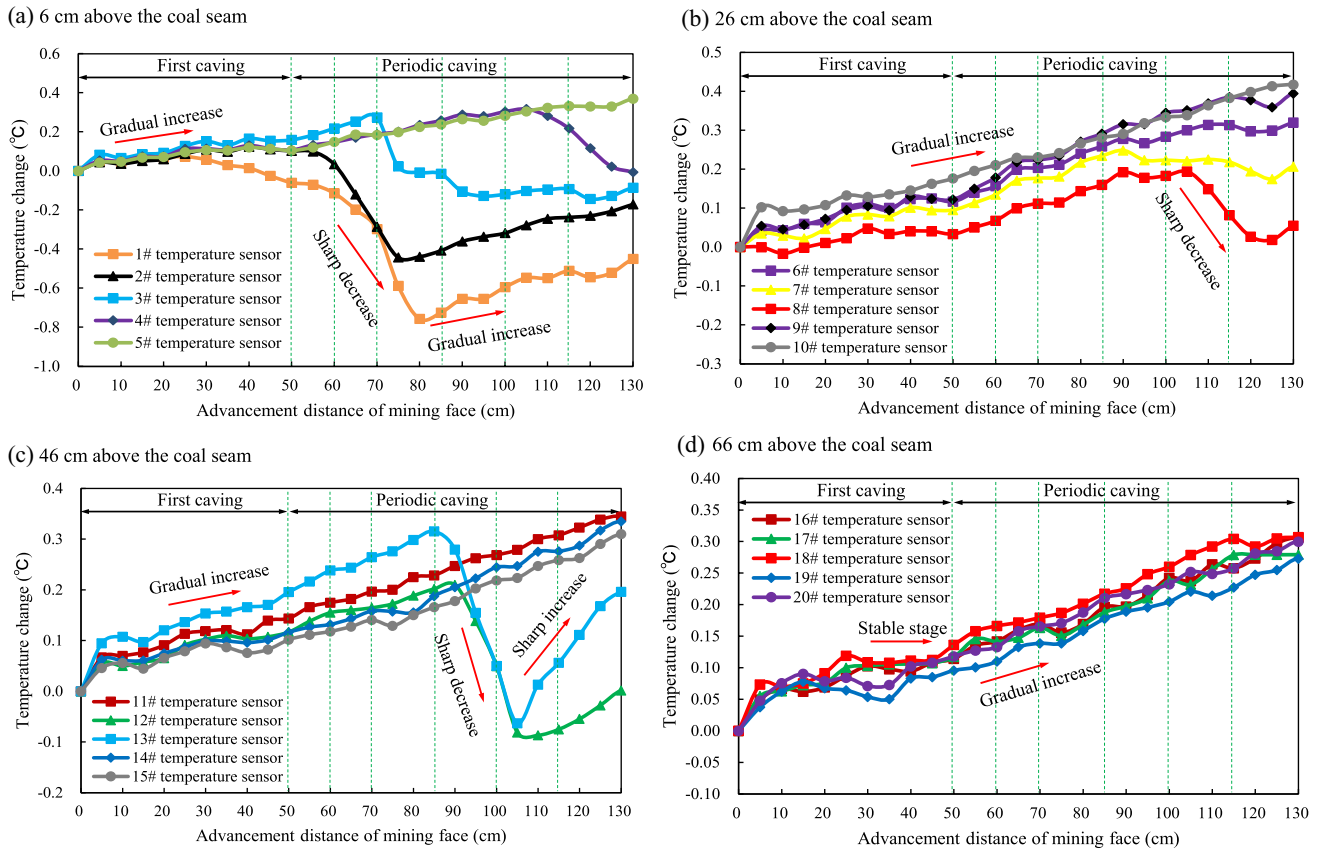
(a) 6 cm above the coal seam
(b) 26 cm above the coal seam
(c) 46 cm above the coal seam
(d) 66 cm above the coal seam

Fig. 11 Overburden rock temperature variation in different height above coal seam

4.1 The interrelation between mining-induced stress and displacement

The mining-induced stress of 1#, 2#, 8#, 9# stress sensors and displacement of overburden rock are selected to analyze the interrelation between the mining-induced stress and

displacement when the mining face advances to 60 cm, 70 cm, 110 cm and 130 cm, as shown in Fig. 12.

During the middle advancement period (60–70 cm) of the mining face, overburden rock appears small scope collapse failure, the distribution of height and width of displacement evolution area shows increase, the mining-induced stress

(a) the mining-induced stress and displacement co-variation with 70 cm mining distance
(b) the mining-induced stress and displacement co-variation with 130 cm mining distance
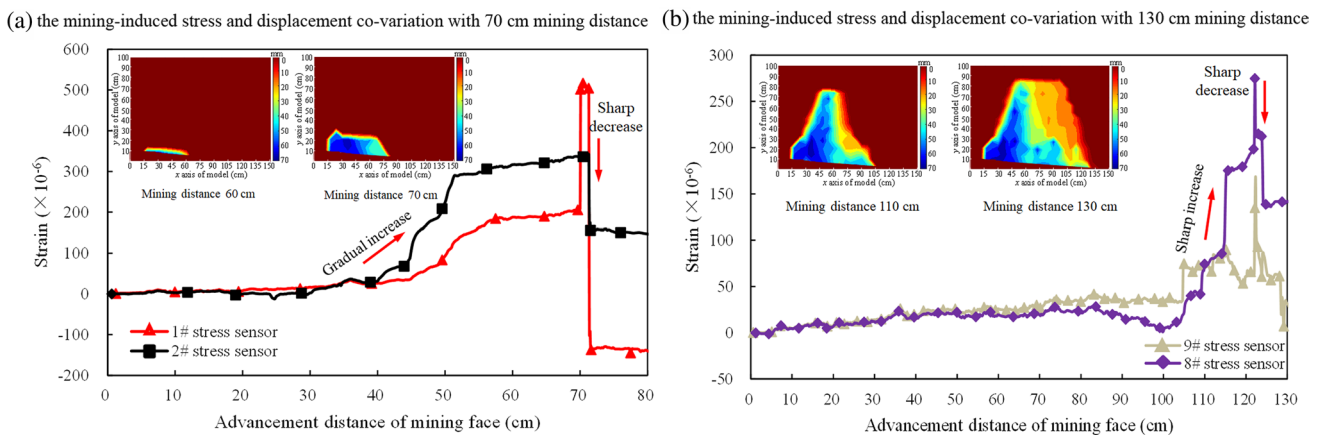
Fig. 12 The mining-induced stress and displacement co-variation characteristic of overburden rock caving zone during coal seam mining
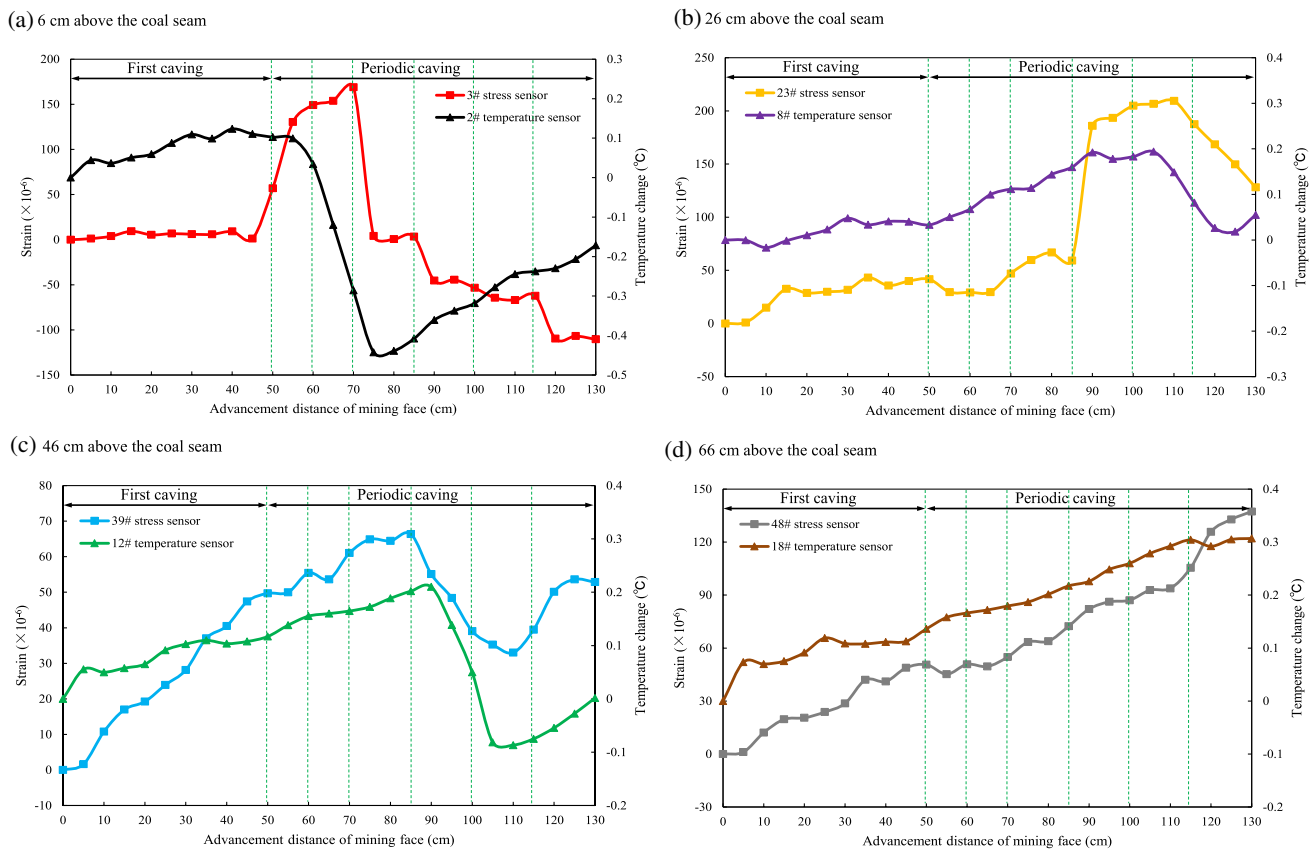
Fig. 13 The mining-induced stress and temperature co-variation characteristic of different overburden rock areas

of 1#, 2# stress sensors both rapidly increase first and then sharply decrease (Fig. 12a). At the later advancement period (110–130 cm) of the mining face, the mining-induced stress of 8#, 9# stress sensors show significant decrease after fluctuating rise and the height and width of displacement evolution area increases rapidly (Fig. 12b).

There is reasonable interrelation between mining-induced stress and displacement of rock strata. The slow increase of displacement and the gradual accumulation of mining-induced stress are in the same process, and the displacement significantly increases when the mining-induced stress shows high-level mutation.

4.2 The interrelation between mining-induced stress and temperature

The first caving of overburden rock mentioned in the manuscript refers to the initial caving phenomenon of rock strata with the same lithology above the coal seam after a certain advancement distance of mining face. The periodic caving refers to the caving phenomenon of rock strata with the same lithology above the coal seam after the first caving. Four groups of sensors in different overburden rock areas are selected to analyze interrelation between mining-induced

stress and temperature. Each group includes one stress sensor and one temperature sensor near the same location in overburden rock, as shown in Fig. 13.

In the fourth stage of overburden rock collapse, the mining-induced stress of the first group sensors shows an obvious stress drop and the temperature also presents significant decrease (Fig. 13a). In the fifth stage of overburden rock collapse, the mining-induced stress of the second group sensors increases significantly and the temperature increases (Fig. 13b), and the mining-induced stress of the third group sensors slightly decreases and the temperature decreases (Fig. 13c). The mining-induced stress and temperature of the fourth group sensors both show steady increase in seven stages of overburden rock collapse (Fig. 13d).

There is good positive interrelation between mining-induced stress and temperature of rock strata. With the increase of mining-induced stress the temperature shows increase, and the temperature presents decreases with the decrease of mining-induced stress. During the advancement process of mining face, the in situ stress of overburden rock changes and the mining-induced stress of rock strata slowly increases, the bending deformation of rock strata leads to deformation energy accumulates and then rock strata temperature gradually increases. When the stress reaches the

(a) overburden rock in caving zone

(b) overburden rock in fracture zone
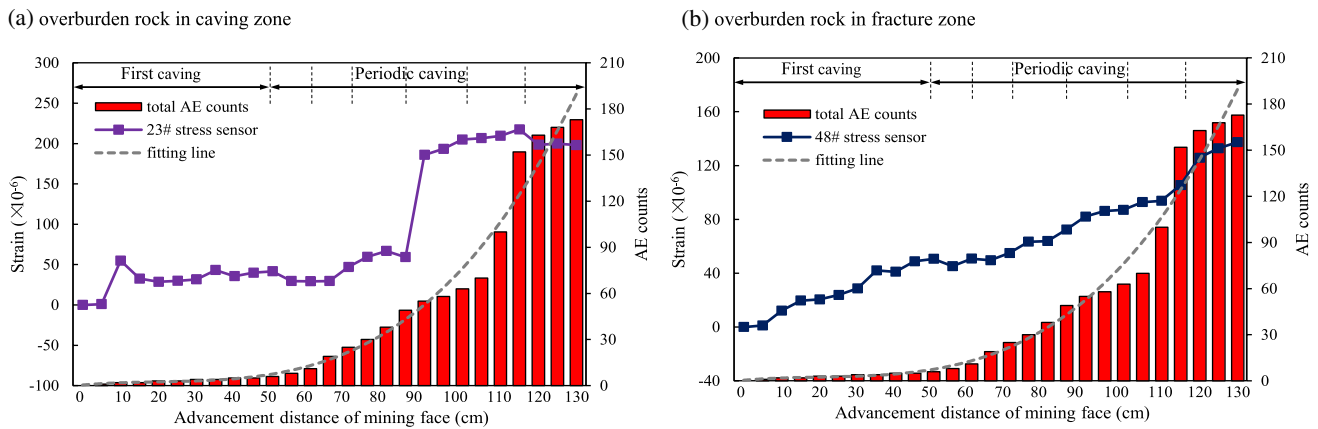
Fig. 14 The mining-induced stress and AE counts co-variation characteristic of overburden rock in different zones

ultimate strength of rock strata, overburden rock occurs collapse and deformation energy is released, and rock strata temperature significantly decreases.

4.3 The interrelation between mining-induced stress and acoustic emission

23#, 48# stress sensors (consistent with the two stress sensors in Sect. 4.2) are selected to analyze the interrelation between mining-induced stress and acoustic emission events, as shown in Fig. 14.

During the first stage of overburden rock collapse (advancement distance 50 cm), the mining-induced stress of two stress sensors shows gradual increase and acoustic emission counts recorded by the acoustic emission monitoring system are stable. During the second stage to the fifth stage of overburden rock collapse (advancement distance 50–100 cm), the mining-induced stress of 23# stress sensor increases sharply (Fig. 14a) and the mining-induced stress of 48# stress sensor shows gentle increase (Fig. 14b), but the acoustic emission counts show significant increase. During the sixth stage to the seventh stages of overburden rock collapse (advancement distance 100–130 cm), the mining-induced stress changes steadily, and the acoustic emission counts increase sharply.

There is still good interrelation between the mining-induced stress and acoustic emission events. The acoustic emission counts increase significantly and mining-induced stress increases in varying magnitudes.

4.4 Characterization of mining-induced stress, displacement, temperature and acoustic emission

The sequence of rock strata collapse can be divided into seven stages during the advancement process of mining

face. Through the analysis of seven stages of rock strata collapse, it can be found that the scope of rock strata collapse area appears alternating cycle phenomenon of "small scale–large scale". The evolution direction of collapse area in seven stages of rock strata collapse develops gradually along the mining face in the horizontal direction, while it develops from lower rock strata to upper rock strata in the vertical direction.

With the transmission and rebalancing of mining-induced stress in the advancement process of mining face, the mining-induced stress has experienced four stages including gentle stability, gradual accumulation, high-level mutation and returning to stability. In addition, the mining-induced stress has synchronous variation characteristics.

The displacement evolution of overburden rock is closely related to its movement. As the advancement of the mining face, the area of rock strata collapse begins to occur at the immediate roof above the coal seam and gradually expands upward to the middle and top of the main roof. During this process, the height and width of overburden rock displacement evolution shows a growing trend and the shape of displacement evolution area presents an inverted funnel. The nonlinear dynamic displacement can be observed from overburden rock local static deformation to overburden rock overall violent collapse.

The overburden rock temperature increment mainly goes through four stages including gradual increase, sharp decrease, sharp increase and gradual increase. From the view of the influence of rock strata temperature change on rock strata collapse stage, the gradual increase stage of temperature occurs in the small scope collapse of rock strata (the first stage and the second stage). The sharp increase stage and gradual increase stage after sharp decrease stage of temperature occurs in the large scope collapse of rock strata (the third stage to the seventh stage). Therefore, the rock masses temperature increment presents slight rise caused

by the stable bending deformation of the rock strata. When overburden rock occurs sudden collapse, the temperature increment will locally drop and rise slowly after fractured overburden rock is compacted.

The location of acoustic emission events is basically consistent with the position of rock strata fracture. The large connected microfracture leads to serious overburden rock collapse along with sharp increase of acoustic emission events. The acoustic emission events massively accumulate appearing in the failure line and ringing count increases dramatically before overburden rock caving.

4.5 Precursor information for overburden rock collapse

During the advancement process of mining face, taking 3# stress sensor and 2# temperature sensor for example, combining with the location of the two sensors (Fig. 6) and overburden rock collapse process (Fig. 7), two sensors remain stable without caving in the first stage of overburden rock collapse when the advancement distance of mining face is 50 cm. Two sensors collapse along with rock strata fracture in the third stage of overburden collapse when the advancement distance of mining face is 70 cm. Therefore, in order to obtain the precursor information of overburden rock collapse, this study mainly considers the evolution characteristics of mining-induced stress, temperature, displacement and acoustic emission ringing count in the before collapse period, during collapse period and post collapse period of overburden rock in the advancement distance of 85 cm,

which provides with some interesting insights about overburden rock collapse, as shown in Fig. 15.

The mining-induced stress has experienced several stages, including stable stage, sharp increase, gradual increase, sharp decrease and then stable stage; the temperature has experienced stable stage, rapid decrease and stable stage; the displacement has experienced slow increase, sharp increase, and stable stage; the acoustic emission ringing counts have experienced slow increase, sharp increase, sharp decrease and relatively stable stage. According to the change characteristics of multiple mechanical parameters, the common causes are analyzed as follows: the stable stage and slow increase of multiple mechanical parameters are caused by slight disturbance of mining activities (advancement distance 0–45 cm); the sharp increase of mining-induced stress, displacement and acoustic emission ringing count are caused by moderate disturbance of mining activities (advancement distance 45–55 cm); the sharp decrease of overburden rock temperature and acoustic emission ringing count are caused by violent disturbance of mining activities (advancement distance 55–70 cm); the subsequent stable stage is caused by the overburden rock being in equilibrium stage again (advancement distance 70–85 cm). Because overburden rock energy has not been released for a long time, the mining-induced stress constantly maintains at high-level. However, overburden rock temperature and acoustic emission ringing count both presents significant drop prior to mining-induced stress abruptly reduces when the mining-induced stress and displacement of rock stratum begin to increase rapidly, the advancement distance of the mining face is determined as the starting point. When the mining-induced
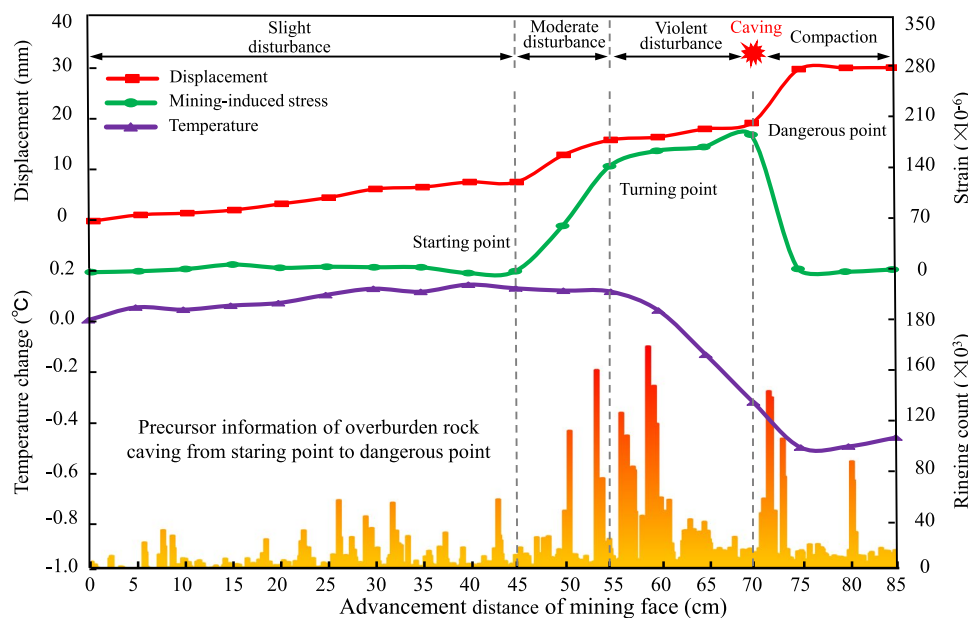
Fig. 15 Comprehensive analysis of mining-induced stress, displacement, temperature and acoustic emission ringing counts in overburden rock collapse

stress and displacement of the rock stratum change from rapidly increasing to slowly increasing and the rock stratum temperature begins to decrease significantly, the advancement distance of the mining face is determined as the turning point. When the rock stratum temperature and acoustic emission ringing counts continue to decrease significantly before the mining-induced stress decreases sharply and the displacement increases suddenly, the advancement distance of the mining face is determined as the dangerous point. The precursor information of overburden rock caving can be obtained from staring point to dangerous point.

In addition, the cause of overburden rock collapse should be further discussed. The phenomenon of overburden rock collapse observed from the experiment occurs after cracks connection. A great many of non-connected micro cracks tend to gradually develop. The spatial distribution of micro crack can be represented by the acoustic emission events position. The internal cause of micro crack development is stress mutation when the stress reaches the ultimate strength. During the development of micro crack, energy will be released leading to temperature rapid reduction, displacement and acoustic emission ringing count sharply increase. Due to overburden rock collapse process is nonlinear dynamic process of stable accumulation and unstable release of deformation energy, mining-induced stress, displacement, temperature and acoustic emission ringing count have changed dramatically before the occurrence of overburden rock collapse, the change law of multiple mechanical parameters is consistent on the general trend and they can be used for reference to each other to predict the overburden rock collapse. Before overburden rock collapse occurs, rock strata temperature obviously decreases and the acoustic emission ringing count surges with the increase of rock displacement and mining-induced stress. Therefore, the collaborative evolution characteristics of mining-induced stress, displacement, temperature increment, acoustic emission ringing count can be identified as the precursor information of overburden rock caving.

4.6 Precursory information warning application for overburden rock collapse

It is concluded that the evolution laws of acoustic emission and electromagnetic radiation have good consistency and the feasibility of synchronous monitoring, and the electromagnetic radiation can be applied to early warn occurrence of coal mine dynamic disasters (Pan et al. 2014; Wang et al. 2018; Qiu et al. 2020). In the manuscript, the monitoring data of electromagnetic radiation obtained from the coal mine site will be used to replace the acoustic emission data to prove the rationality of the precursor information of dynamic disasters. The electromagnetic radiation monitoring point is located on the upper side of the haulage gateway, and 60 m ahead from 21221 mining face. The position of the electromagnetic radiation point would move forward with the advancement of 21221 mining face, and always maintain the original monitoring distance from mining face. The threshold value of electromagnetic radiation intensity is 35 mV. Figure 16 showed the variation characteristics of electromagnetic radiation intensity and single support resistance during the tunneling of 21221 mining face ventilation roadway from March to April 2011, and the fluctuation law of electromagnetic
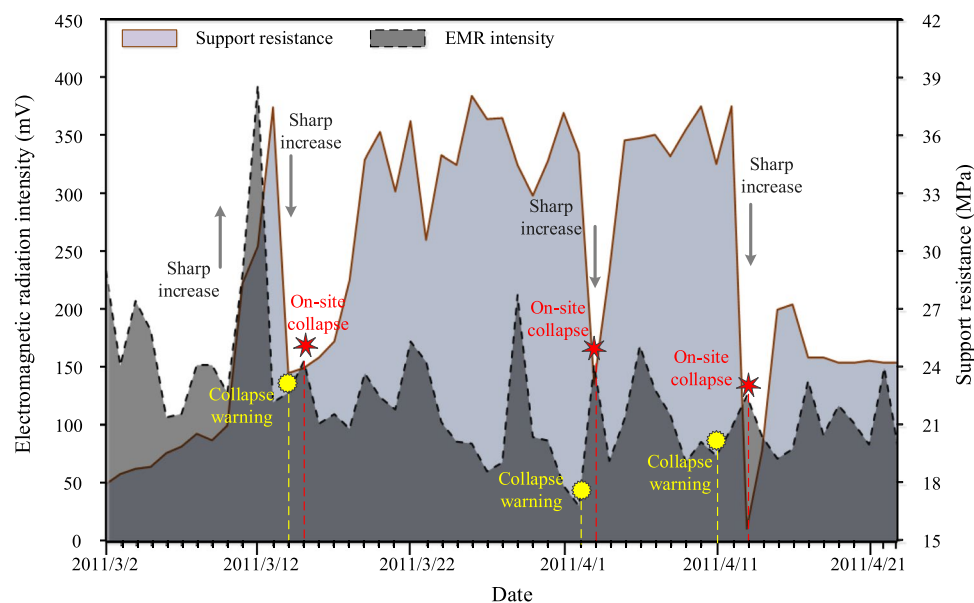
Fig. 16 Characteristics of electromagnetic radiation and support resistance in 21221 mining face in Qianqiu coal mine (in 2011)

radiation intensity and support resistance presented good consistency.

During the period from March 11, 2011 to March 13, 2011, the peak of support resistance was 37.4 MPa, and the electromagnetic radiation intensity reached the maximum value of 392 mV at the same time, then both of them rapidly decreased almost simultaneously. During the period from March 18, 2011 to April 21, 2011, the electromagnetic radiation intensity and support resistance basically remained high level, while there was a significant sharp decrease in April 3, 2011 and April 11, 2011 respectively. According to the synchronous and sharp change characteristics of multiple mechanical parameters in the previous section, it was regarded as the precursor information of overburden rock collapse. Therefore, the date of synchronous and rapid decrease of electromagnetic radiation intensity and support resistance was taken as the early warning time of overburden rock collapse, namely, March 14, 2011, April 2, 2011 and April 11, 2011. There was the fact that the actual date of overburden rock collapse on site was the day after the warning date, and it could be confirmed that the precursor information of synchronous and sharp change characteristics of multiple mechanical parameters had certain reliability and accuracy. It is worth noting that there were some differences between experimental results and on-site monitoring results, mainly reflected in differences in monitoring scales, stress and deformation conditions, but both could describe and summarize the evolution characteristics in the same phenomenon.

It should be noted that overburden rock collapse process is random and sudden and the failure forms are various. It is obviously unreliable to predict overburden rock collapse by adopting only one monitoring method. Because the mechanism of the overburden rock collapse induced by the mining effect is extremely complex, the multiple mechanical parameters change characteristics and precursor information will be not same for different condition including coal seam, overburden rock structure, mining method and other factors. On the basis of analyzing the geological condition, mining technology and strata behavior law and other influencing factors, a comprehensive prediction study of multiple mechanical parameters of overburden rock collapse process should be carried out. Therefore, the research methods and conclusions in this study are only a kind of exploration, hoping to provide some reference for the control methods of overburden rock caving.

5 Conclusions

Based on the 21221 mining face geological condition of Qianqiu coal mine in Henan Province, China, a physical model integrated a new multiple mechanical parameters monitoring system is constructed to simulates the overburden rock deformation and collapse process. The interrelation and evolution characterization of mining-induced stress, displacement, temperature and acoustic emission events of overburden rock collapse behavior is reported and discussed in this paper. The main conclusions drawn from this study are summarized below.

(1) The scale of overburden rock caving area appears alternating cycle phenomenon of "small scale–large scale". The advancement distance of mining face is 10 cm or 15 cm when the overburden rock occurs multiple collapse stages except for the first collapse stage. Although overburden rock caving interval is nearly uniform, the main characteristic is uneven caving strength.

(2) The mining-induced stress has synchronous variation characteristics. The mining-induced stress of rock strata near the gob has experienced four stages including gentle stability, gradual accumulation, high-level mutation and returning to stability. The nonlinear dynamic displacement of rock strata can be observed from local static deformation to overall violent collapse. The slow increase of displacement and the gradual accumulation of mining-induced stress are in the same process, and the displacement significantly increases when the mining-induced stress shows high-level mutation.

(3) The rock masses temperature increment presents slight rise caused by the stable bending deformation of the rock strata. When overburden rock occurs sudden collapse, the temperature increment will locally drop and rise slowly after fractured overburden rock is compacted. The temperature increment shows increase with the increase of the mining-induced stress and it presents decrease with the decrease of the mining-induced stress. The acoustic emission events massively accumulate along the failure line of collapsed rock strata. The variation of other mechanical parameters is not synergetic with the significant change of mining-induced stress.

(4) The mining-induced stress shows reasonable and reliable interrelation with displacement, temperature and acoustic emission events. Before overburden rock collapse occurs, rock temperature increment decreases and the acoustic emission ringing counts surges with the increase of displacement and mining-induced stress. The collaborative characteristics of multiple mechanical parameters can be identified as the precursor information of overburden rock caving.

Declarations

Conflict of interest No conflict of interest exits in the submission of the manuscript, and manuscript is approved by all authors for publication.

References

Alejano LR, Taboada J, García-Bastante F, Rodriguez P (2008) Multi-approach back-analysis of a roof bed collapse in a mining room excavated in stratified rock. Int J Rock Mech Min Sci 45(6):899–913

Amini M, Sarfaraz H, Esmaeili K (2018) Stability analysis of slopes with a potential of slide-head-toppling failure. Int J Rock Mech Min Sci 112:108–121

Bai QS, Tu SH, Wang FT, Zhang C (2017) Field and numerical investigations of gateroad system failure induced by hard roofs in a longwall top coal caving face. Int J Coal Geol 173:176–199

Chen DD, He FL, Xie SR, Zeng JC (2019) Time-space relationship between periodic fracture of plate structure of main roof and rebound in whole region with elastic foundation boundary. Chin J Rock Mech Eng 38(06):1172–1187

Cheng ZB, Kong DZ, Yang JH (2016) The breaking characteristics of thick hard roof and determination of support capacity in fully mechanized caving face. J Min Sci Technol 1(2):172–180

Ding WJ, Zhou ZH, Liu J, Tk H, Wang JX, Li J, Zhang X (2022) Research on the identification of precursor information of limestone rock burst under triaxial unloading conditions. Geofluids 2022:3282276

Dou LM, He XQ, He H, He J, Fan J (2014) Spatial structure evolution of overlying strata and inducing mechanism of rock burst in coal mine. T Nonferr Metal Soc 4:1255–1261

Gao FQ, Stead D, Kang HP, Wu YZ (2014a) Discrete element modelling of deformation and damage of a roadway driven along an unstable goaf: a case study. Int J Coal Geol 127:100–110

Gao Y, Zhang QS, Li SC, Jiang YJ (2014b) An experiment of temperature field of rock mass near water-bearing structure during roadway excavation. J Cent South Univ T 45(2):550–556

Ghabraie B, Ren G, Zhang XY, Smith J (2015) Physical modelling of subsidence from sequential extraction of partially overlapping longwall panels and study of substrata movement characteristics. Int J Coal Geol 140:71–83

Gong WL, Wang J, Liu DQ (2016) Infrared thermography for geomechanical model test. Science Press

Hao TX, Li F, Tang YJ, Zhao LZ, Wang ZH (2022) Infrared precursor of pre-cracked coal failure based on critical slowing down. Geomat Nat Haz Risk 13(1):1682–1699

He MC, Jia XN, Gong WL, Faramarzi L (2010) Physical modeling of an underground roadway excavation in vertically stratified rock using infrared thermography. Int J Rock Mech Min Sci 47(7):1212–1221

Jiang YD, Zhao YX (2015K) State of the art: investigation on mechanism, forecast and control of coal bumps in China. Chin J Rock Mech Eng 34(11):2188–2204

Jiang YD, Pan YS, Jiang FX, Dou LM, Ju Y (2014) State of the art review on mechanism and prevention of coal bumps in China. J China Coal Soc 39(2):205–213

Khan M, He XQ, Farid A, Song DZ, Li ZL, Tian XH, Ni MQ (2021) A novel geophysical method for fractures mapping and risk zones identification in a coal mine, Northeast, China. Energy Rep 7:3785–3804

Kumar R, Singh AK, Mishra AK, Singh R (2015) Underground mining of thick coal seams. Int J Min Sci Technol 25(6):885–896

Li SC, Gao CL, Zhou ZQ, Li LP, Wang MX, Yuan YC, Wang J (2019) Analysis on the precursor information of water inrush in karst tunnels: a true triaxial model test study. Rock Mech Rock Eng 52:373–384

Li HG, Li HM (2017) Mechanical properties and acoustic emission characteristics of thick hard roof sandstone in Shendong coal field. Int J Coal Sci Technol 4:147–158

Liao Z, Feng T, Yu WJ, Wu GS, Li K, Gong FQ (2020) Experimental and theoretical investigation of overburden failure law of fully mechanized work face in steep coal seam. Adv Civ Eng 2020:8843172

Lin Q, Labuz JF (2013) Fracture of sandstone characterized by digital image correlation. Int J Rock Mech Min Sci 60:235–245

Liu WG (2011) Underground pressure characteristic and roof disaster mechanism of shallow buried full-mechanized mining field with large mining-height. Coal Min Technol 16(5):73–76

Liu YK, Zhou FB, Liu L, Liu C, Hu SY (2011) An experimental and numerical investigation on the deformation of overlying coal seams above double-seam extraction for controlling coal mine methane emissions. Int J Coal Geol 87(2):139–149

Liu JB, Song ZM, Chen SM, Lian YX, Yang XN, Qu YW (2017) Main mineable coal seam gas geological pattern in Xiaoxiong Structural Belt, Henan Province. Coal Geol China 29(2):35–39

Liu SH, Pan JF, Xia YX (2019) Study on induced mechanism of rock bursts by fracture movement of hard magmatic beds. Chin J Rock Mech Eng 38(3):499–510

Lou JF, Gao FQ, Yang JH, Ren YF, Li JZ, Wang XQ, Yang L (2021) Characteristics of evolution of mining-induced stress field in the longwall panel: insights from physical modeling. Int J Coal Sci Technol 8:938–955

Lv JG, Jiang YD, Li SG, Ren SD, Jiang WZ, Zhang ZC (2014) Characteristics and mechanism research of coal bumps induced by faults based on extra thick and hard roof. J China Coal Soc 39(10):1961–1969

Mao LT, Zhu XX, An LQ, Cai GS, Hao N (2013) Application of digital target marker image correlation method in model experiment. J Liaoning Technical Univ 32(10):1367–1373

Mao LT, Hao N, An LQ, Chiang FP, Liu HB (2015) 3D mapping of carbon dioxide-induced strain in coal using digital volumetric speckle photography technique and X-ray computer tomography. Int J Coal Geol 147–148:115–125

Munoz H, Taheri A, Chanda EK (2016) Pre-peak and post-peak rock strain characteristics during uniaxial compression by 3D digital image correlation. Rock Mech Rock Eng 49(7):2541–2554

Pan DW, Liu XF, Wang EY, Yuan GH, Xu JB, Wang SH (2014) ULF electromagnetic radiation response on mining activity in the coal seam with outburst risk. Saf Environ Eng 21(4):148–151+158

Qi QX, Li YZ, Zhao SK, Zhang NB, Zheng WY, Li HT, Li HY (2019) Seventy years development of coal mine rock burst in China: establishment and consideration of theory and technology system. Coal Sci Technol 47(9):1–40

Qian MG, Xu JL (2019) Behaviors of strata movement in coal mining. J China Coal Soc 44(4):973–984

Qiu LM, Liu ZT, Wang EY, He XQ, Feng JJ, Li BL (2020) Early-warning of rock burst in coal mine by low-frequency electromagnetic radiation. Eng Geol 279:105755

Ren YF, Li ZJ (2019) Experimental study on time series character of roof cutting in shallow working face. J China Coal Soc 44(S2):399–409

Shabanimashcool M, Li CC (2015) Analytical approaches for studying the stability of laminated roof strata. Int J Rock Mech Min Sci 79:99–108

Shan RI, Huang B, Song YW, Wu HM, Fu XL (2016) Ground pressure features of roadway under close range goaf in the Xinyu Mine. J Min Sci Technol 1(1):29–37

Shen B, King A, Guo H (2008) Displacement, stress and seismicity in roadway roofs during mining-induced failure. Int J Rock Mech Min Sci 45(5):672–688

Shen WL, Bai JB, Wang XY, Yu Y (2016) Response and control technology for entry loaded by mining abutment stress of a thick hard roof. Int J Rock Mech Min Sci 90:26–34

Singh GSP, Singh UK (2010) Numerical modeling study of the effect of some critical parameters on caving behavior of strata and support performance in a longwall working. Rock Mech Rock Eng 43(4):475–489

Song ZQ, Hao J, Shi YK, Tang JQ, Liu JK (2019) An overview of connotation and development of practical ground pressure control theory. J Shandong Univ Sci Technol 38(1):1–15

Su GS, Zhao GF, Jiang JQ, Hu XC (2021) Experimental study on the characteristics of microseismic signals generated during granite rockburst events. B Eng Geol Environ 80(8):6023–6045

Sun XM, Chen F, Miao CY, Song P, Li G, Zhao CW, Xia X (2018) Physical modeling of deformation failure mechanism of surrounding rocks for the deep-buried tunnel in soft rock strata during the excavation. Tunn Undergr Space Technol 74:247–261

Tsesarsky M (2012) Deformation mechanisms and stability analysis of undermined sedimentary rocks in the shallow subsurface. Eng Geol 133–134:16–29

Wang HW, Jiang YD, Xue S, Mao LT, Lin ZN, Deng DX, Zhang DQ (2016) Influence of fault slip on mining-induced pressure and optimization of roadway support design in fault-influenced zone. J Rock Mech Geotech Eng 8(5):660–671

Wang HW, Jiang YD, Deng DX, Zhang DQ, Lv JG, Zeng XT (2017) Investigation on the inducing factors of coal bursts under complicated geological environment in Yima mining area. Chin J Rock Mech Eng 36(S2):4085–4092

Wang EY, Liu XF, He XQ, Li ZH (2018) Acoustic emission and electromagnetic radiation synchronized monitoring technology and early-warning application for coal and rock dynamic disaster. J Chin Univ Min Technol 47(5):942–948

Wang HW, Shi RM, Lu CS, Jiang YD, Deng DX, Zhang DQ (2019) Investigation of sudden faults instability induced by coal mining. Saf Sci 115:256–264

Wang HW, Shi RM, Deng DX, Jiang YD, Wang G, Gong WL (2020a) Characteristic of stress evolution on fault surface and coal bursts mechanism during the extraction of longwall face in Yima mining area. China J Struct Geol 136:104071

Wang HW, Xue S, Shi RM, Jiang YD, Gong WL, Mao LT (2020b) Investigation of fault displacement evolution during extraction in longwall panel in an underground coal mine. Rock Mech Rock Eng 53:1809–1826

Wang CL, Cao C, Liu YB, Li CF, Li GY, Lu H (2021a) Experimental investigation on synergetic prediction of rock burst using the dominant-frequency entropy of acoustic emission. Nat Hazards 108(3):3253–3270

Wang HW, Deng DX, Shi RM, Yang GZ, Xu S, Jiang YD (2021b) Investigation on the movement and fracture characteristics of an extra-thick hard roof during longwall panel extraction in the Yima mining area. China Geofluids 2021:4092242

Wang HW, Shi RM, Song JQ, Tian Z, Deng DX, Jiang YD (2021c) Mechanical model for the calculation of stress distribution on fault surface during the underground coal seam mining. Int J Rock Mech Min Sci 144:104765

Wang JX, Wang EY, Yang WX, Li BL, Li ZH, Liu XF (2022) Rock burst monitoring and early warning under uncertainty based on multi-information fusion approach. Measurement 205:112188

Xie HB, Xu YF, Kang JW (2008) Relationship between vitrinite reflectance of deformed coal and palaeo tectonic stress field in western Henan coalfield. Coal Geol Explor 36(4):1–4

Yuan L, Jiang YD, He XQ, Dou LM, Zhao YX, Zhao XS, Wang K, Yu Q, Lu XM, Li HC (2018) Research progress of precise risk accurate identification and monitoring early warning on typical dynamic disasters in coal mine. J China Coal Soc 43(2):306–318

Zhang QS, Gao Y, Li SC, Li LP, Yuan XS, Zhao JG, Li ZP (2011) Similarity simulation study of temperature response feature of rock mass affected by mining around water-bearing structure. Chin J Rock Mech Eng 30(07):1356–1362

Zhu WS, Li Y, Li SC, Wang SG, Zhang QB (2011) Quasi-three-dimensional physical model tests on a cavern complex under high in-situ stresses. Int J Rock Mech Min Sci 48(2):199–209